INTERNATIONAL ATOMIC ENERGY AGENCY
UNITED NATIONS EDUCATIONAL, SCIENTIFIC AND CULTURAL ORGANIZATION

INTERNATIONAL CENTRE FOR THEORETICAL PHYSICS
34100 TRIESTE (ITALY) - P.O.B. 586 - MIRAMARE - STRADA COSTIERA 11 - TELEPHONE: 2240-1
CABLE: CENTRATOM - TELEX 460392 - I

SMR/459-6

SPRING COLLEGE IN CONDENSED MATTER ON 'PHYSICS OF LOW-DIMENSIONAL STRUCTURES' (23 April - 15 June 1990)

BACKGROUND MATERIAL

G. BASTARD
Département de Physique ENS
24 Rue L'homond
F-75005 Paris
France

CHAPTER III

Envelope function description of heterostructure electronic states

I. Introduction.

From Chapter II we know which are the eigenstates of bulk III-V compounds in the vicinity of the zone centre. In this chapter we shall deal with the determination of the eigenstates in heterostructures. The emphasis will be placed on a simple description of these eigenstates, i.e. a description based on the Kane analysis of the dispersion relations of the host materials. In this envelope function description [1-5], our problem will be to find the boundary conditions which the slowly varying parts of the heterostructure wavefunctions must fullfil at the hetero-interfaces.

It should be stressed that other approaches to the heterostructure energy levels have been proposed which are more microscopic in essence than the envelope function scheme. In the empirical tight-binding calculations for instance (see e.g. [6]), one begins with a series of energies which are characteristic of the sp^3 bonds linking one atom to its neighbours. The heterostructure wavefunction is then built atom after atom. In other words a heterostructure is nothing but a bulk material with a very large unit cell (e.g. the superlattice unit cell in the case of a periodic stacking of the A and B layers). It was previously thought that the size of the computer calculations necessary to handle such large cells would become rapidly prohibitive, restricting the tight-binding analysis to short period superlattices where the unit cell is not too large. Chang and Schulman have however shown how to cure this drawback [7] and the tight-binding model is nowadays successfully used for heterostructures of any size, although it may have difficulties in handling self-consistent calculations which arise when charges are present in the heterostructure.

Another microscopic approach is the pseudo-potential formalism, which is very sucessful in bulk materials. Recently, it has been applied to a variety of heterostructures by Jaros *et al.* [8, 9]. Here, the core of the model is to consider, say, a periodic stacking of GaAs and AlAs slabs as a perturbation over the zero-order situation, which in this case would be the bulk GaAs. In other words a calculation is made analogous to the deep level ones in bulk semiconductors. The advantage of these microscopic approaches is their capacity to handle any heterostructure energy levels, i.e. those close to or far from the Γ edge. This occurs because these models reproduce the whole bulk dispersion relations. The model that we shall develop has no such generality. Basically, it is restricted to the vicinity of the high-symmetry points in the host's Brillouin zone (Γ, X, L). We feel however that it is invaluable due to its simplicity and versatility. If often leads to analytical results and leaves the user with the feeling that he can trace back, in a relatively transparent way, the physical origin of the numerical results. Besides, most of the heterostructures' energy levels

relevant to actual devices are relatively close to a high symmetry point in the hosts' Brillouin zone.

We shall first present the assumptions used to derive the envelope function model. As the reader may have perceived in chapter II, the algebra is relatively easy when the in-plane wavevector $\boldsymbol{k}_{\_}$ of the carrier is zero. The heterostructure states can then be classified according to m_J, the z projection of the total angular momentum $\boldsymbol{J}$, and two kinds of energy levels result. The first kind corresponds to light particle states which are hybrids of the Γ_6, Γ_8^l and Γ_7 host states, whereas the second kind corresponds to the heavy hole levels. These $\boldsymbol{k}_{\_} = \boldsymbol{0}$ states in quantum wells and superlattices will be extensively discussed and our considerations will be illustrated by specific examples. The third part of this chapter will be devoted to a discussion of the in-plane dispersion relations in the heterostructures. This is a topic which is currently being actively researched. Because of the mixing between the $\boldsymbol{k}_{\_} = \boldsymbol{0}$ light and heavy particle states it has proved, up to now, impossible to obtain analytical solutions of the $\boldsymbol{k}_{\_} \neq \boldsymbol{0}$ heterostructure problem. Therefore, we shall only present the assumptions used for the calculations and some examples of the in-plane dispersion relations in several heterostructures. Unless otherwise specified, the heterostructures are assumed to be under flat band conditions, i.e. contain no charges. In the presence of charges, self consistent calculations of energy levels are required. They are the subject of chapter V.

II. The envelope function model.

II.1 PRELIMINARIES. — Advanced epitaxial techniques, such as molecular beam expitaxy or metal-organic chemical vapour deposition, have made it possible to grow interfaces between two semiconductors which are flat up to one atomic monolayer (2.83 Å in GaAs), which is the ultimate resolution which can be achieved. It is common to represent such an ideal interface in terms of a continuously varying position-dependent band edge (Fig. 1). Basically speaking the sketch shown in figure 1 means that for $z \gg 0$ the electron experiences a one-electron potential which is identical to that of a perfect bulk A material, whereas for $z \ll 0$ it experiences a one-electron potential which is the same as is found in a perfect bulk B layer. Of course, this scheme that we shall follow later on is only approximately true. Its accuracy is limited by several factors, both fundamental and technological in origin. On the one hand the sketch shown in figure 1 by-passes any ambiguity concerning the description of the electron states which originates from the border atoms, i.e. that hybrid interface bonds exist which are present in neither the bulk A layer nor in the bulk B layer. On the other hand, figure 1 tacitly assumes a perfectly bi-dimensional growth, i.e. that all over the area S the structure grows monolayer after monolayer. This bi-dimensional growth is, in practice never completely achieved and for that reason the interface location along the z axis varies with the in-plane coordinates. In practice, we feel it is better to envisage the interface as having a finite thickness to account for the effects previously mentioned. Fortunately, most of the electronic states which we shall discuss in the rest of the book hardly experience the interfaces, as they have small probability amplitudes of being found in these regions. Thus, in a first

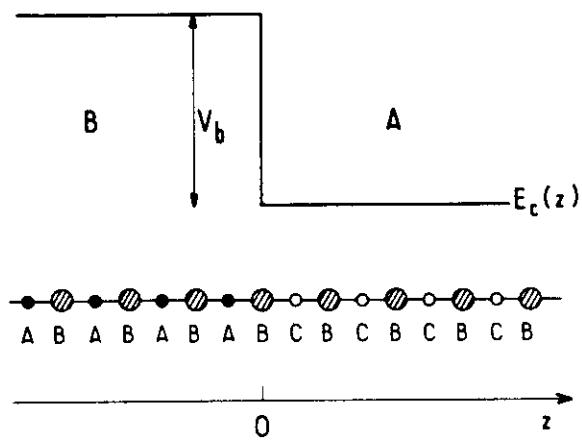

Fig. 1. — One-dimensional sketch of a heterojunction formed between two perfectly lattice-matched A and B semiconductors with chemical formulae CB and AB respectively. Upper part : representation in terms of a position-dependent conduction band edge. Lower part : actual bonds. Notice the formation of the hybrid bonds A-B-C at the interface.

approximation and for technologically abrupt interfaces, we shall retain the notion of mathematically abrupt interfaces. Consequences of the deviations in the actual interfaces with respect to this idealized model will be examined in chapter IV.

For certain heterostructures, the notion of abrupt interfaces is irrelevant from the growth point of view due, for example, to an excessive and uncontrolled interdiffusion between the A and B materials. For those heterostructures with severely graded interfaces, one should resort to modelization of the grading effect. To our knowledge, little effort has been devoted to this technologically important problem.

Since the notion of interfaces is somewhat fuzzy, the definition of layer thickness is also rather imprecise. However in the case of periodically arranged heterostructures (superlattices) the X-ray determination of the superlattice period is precise (see e.g. [10]). On the other hand, the thickness of an individual layer is rarely known to an accuracy of more than one atomic monolayer. In-situ measurements such as Reflection High Energy Electron Diffraction oscillations [11] have proved to be very valuable in ascertaining the layer thickness. Simpler techniques such as measuring the growth duration and using calibration obtained on thick (~ 1 μm) layers are less precise for the narrow layers (~ 100 Å) which interest us.

The abrupt interface model sketched in figure 1 makes a clear distinction between barrier-acting (B) and well-acting (A) materials. One may however raise questions on the significance of barrier and well denominations since we have seen that the interface notion is not very well defined. The two notions call for different properties. The interface is ill-defined because it is difficult to know at the atomic scale what kind of environement an electron sees when it is in the transition region between the A and B layers. The notion of wells and barriers calls, on the contrary, for the asymptotic behaviour of the carrier wavefunction occurring far from the

interface. The exact heterostructure wavefunction corresponding to ε_p where $0 \leq \varepsilon_p \leq V_b$ oscillates deep in the A layer but is exponentially damped in the B layer. On the other hand if $\varepsilon_p \geq V_b$, the wavefunction would oscillate in both kinds of layers.

With respect to the valence and conduction edges, two possible band edge profiles exist for an AB heterostructure. In figure 2a B is a barrier for both the valence and conduction electrons (type I configuration). Another situation is also found (type II, also called staggered configuration) where one material acts as a well for conduction electrons but as a barrier for valence electrons (Fig. 2b). Examples of the type I configuration are GaAs-Ga(Al)As, $Ga_{0.47}Al_{0.53}As$-InP, GaSb-AlSb etc.... whereas InAs-GaSb is an example of a heterostructure which diplays a type II configuration.

II.2 THE ENVELOPE FUNCTION FRAMEWORK. — In the following we shall assume that the A and B materials constituting the heterostructures are perfectly lattice-matched and that they crystallize with the same cristallographic structure (in most cases the zinc-blende structure). The approximation of perfect lattice matching is relatively well justified for GaAs-Ga(Al)As and $Ga_{0.47}In_{0.53}As$-InP (if the In mole

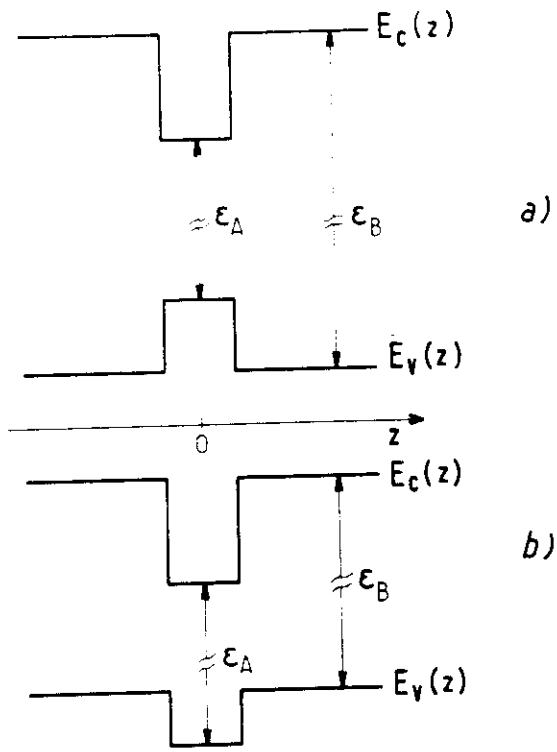

Fig. 2. — Conduction and valence band profiles in a type I heterostructure (Fig 2a) and in a type II heterostructure (Fig. 2b).

fraction is really 0.53) : the relative lattice mismatch $\delta a/a = (a_B - a_A)/a_A$ between both host materials is between 0 and 0.1 %. For other materials (e.g. GaSb-AlSb) $\delta a/a$ is too large ($\geq$ 0.6 %) to be neglected. If the layers constituting the heterostructures are thin enough, the lattice mismatch is accomodated by strain and stress effects in each kind of layer in order to achieve a common in-plane lattice parameter [12-14]. The envelope function framework can be suitably generalized to include the stress effects. We shall not discuss these effects here, as [12-14] can be referred to for such a generalization.

In the envelope function model the similarity found between the Kane matrix elements of the various III-V or II-VI compounds is exploited. Two key assumptions are made :

i) Inside each layer the wavefunction is expanded on the periodic parts of the Bloch functions of the edges under consideration

$$\psi(\boldsymbol{r}) = \sum_l f_l^{(A)}(\boldsymbol{r})\, u_{l,\boldsymbol{k}_0}^{(A)}(\boldsymbol{r}) \tag{1}$$

if $\boldsymbol{r}$ corresponds to an A layer and,

$$\psi(\boldsymbol{r}) = \sum_l f_l^{(B)}(\boldsymbol{k})\, u_{l,\boldsymbol{k}_0}^{(B)}(\boldsymbol{r}) \tag{2}$$

if $\boldsymbol{r}$ corresponds to a B layer. In equations (1, 2), $\boldsymbol{k}_0$ is the point in the Brillouin zone around which the heterostructure states are built. The summation over l runs over as many edges as are included in the analysis.

ii) The periodic parts of the Bloch functions are assumed to be the same in each kind of layer which constitutes the heterostructure :

$$u_{l,\boldsymbol{k}_0}^{(A)}(\boldsymbol{r}) \equiv u_{l,\boldsymbol{k}_0}^{(B)}(\boldsymbol{r}). \tag{3}$$

Thus our heterostructure wavefunction will be written as

$$\psi(\boldsymbol{r}) = \sum_l f_l^{(A,B)}(\boldsymbol{r})\, u_{l,\boldsymbol{k}_0}(\boldsymbol{r}) \tag{4}$$

and our objective will be to determine $f_l^{(A,B)}(\boldsymbol{r})$. But let us first examine some of the implications of assumptions (i) and (ii).

The fact that we have truncated the summation over l to a finite number of band edges means that we have tacitly assumed that the heterostructure states are built with the host wavevectors $\boldsymbol{k}_A$, $\boldsymbol{k}_B$ which, when measured from $\boldsymbol{k}_0$, are small. More precisely this means that the ranges $\delta k_A = |\boldsymbol{k}_A - \boldsymbol{k}_0|$, $\delta k_B = |\boldsymbol{k}_B - \boldsymbol{k}_0|$ which are required to build $\psi(\boldsymbol{r})$ are such that the actual dispersion relations of the hosts are well described by the approximate $\varepsilon_l^{(A)}(\boldsymbol{k}_A)$, $\varepsilon_l^{(B)}(\boldsymbol{k}_B)$. The latter result from the diagonalization of the $\delta\boldsymbol{k}.\boldsymbol{p}$ bulk Hamiltonians inside the restricted set of edges retained in equations (1, 2). To discover such a range, one should (in principle) compare the approximate $\varepsilon_l^{(A)}(\boldsymbol{k}_A)$, $\varepsilon_l^{(B)}(\boldsymbol{k}_B)$ with more exact computations. Such a

comparison has been made for the GaAs-AlAs pair in the previous chapter where the results of the Kane model, designed to be valid in the vicinity of the zone centre, were compared to a tight binding calculation [15] valid over the whole Brillouin zone. This comparison demonstrates that the conduction band states are fairly well reproduced by the Kane model in *both* GaAs and AlAs materials up to ~ 0.3 eV in the GaAs conduction band. Valence states are reproduced with comparable accuracy.

As the summations over l in equations (1, 2) are the same for both the A and B layers, it is assumed that the heterostructure state is built from $\boldsymbol{k}_A$, $\boldsymbol{k}_B$ wavevectors close to the same $\boldsymbol{k}_0$ edge in each layer. To illustrate this point we shall suppose that we want to apply the envelope function model to a GaAs-AlAs quantum well grown along the [001] direction. Let us set $k_x = k_y = 0$. The model will give results for the energy levels related to either the Γ extremum ($\boldsymbol{k}_0 = \boldsymbol{0}$) or to the X extremum $\left(\boldsymbol{k}_0 = \left(0, 0, \frac{2\pi}{a_0}\right)\right)$ *separately*. The upper lying valence states will always be Γ-like and essentially confined in GaAs. The lowest lying-conduction states will be Γ-like if the GaAs well is wide enough. Some of the excited conduction states will be Γ-like whereas others will be X-like. If the GaAs well is narrow enough the lowest lying Γ states will coincide in energy with the lowest lying X state (this is because the X band has a much heavier mass along the [001] axis than the Γ mass). The envelope function scheme will predict that these two states are degenerate in energy and consequently will fail. The degeneracy is actually lifted and the two levels anticross which leads to a strong mixing between the Γ-related and X-related wavefunctions. More generally, for heterostructures which are such that the widely separated extrema of the host Brillouin zone are involved in the heterostructure wavefunctions, the envelope function model will, in essence, be unable to account for the couplings between the various valleys. To fully describe the latters, models involving the entire hosts' Brillouin zones will be required, e.g. tight-binding [6-7] or pseudo-potential methods [8-9]. On the other hand, for heterostructure states which are built from the same extrema in both types of layers, the envelope function model should work well. It has been successfully implemented for the Γ-related states of a variety of III-V heterostructures : GaAs-Ga(Al)As, $Ga_{0.47}In_{0.53}As$-InP, GaSb-InAs... as well as for the L-related states of PbTe-Pb(Sn)Te heterostructures (see [16] for more details). From now on we shall restrict our considerations to the Γ-related extrema.

The assumption of identical $u_{l,0}^{(A)}(\boldsymbol{r})$, $u_{l,0}^{(B)}(\boldsymbol{r})$ implies that the interband p_x matrix element $\langle S|p_x|X\rangle$ is the same in the A and B layers. Let the plane $z = z_0$ be the interface separating the A and B layers (the growth axis is assumed to be the z axis). Since the $u_{l,0}$ are linearly independent and since $\psi(\boldsymbol{r})$ has to be continuous at $z = z_0$ it results that

$$f_l^{(A)}(\boldsymbol{r}_\perp, z_0) = f_l^{(B)}(\boldsymbol{r}_\perp, z_0) \tag{5}$$

where $\boldsymbol{r}_\perp$ is a two-dimensional position vector. Since the lattice constants of the host layers are assumed to be the same (at least in the layer plane in order to include the strained layer materials in our analysis), the heterostructure becomes translationally

invariant in the layer plane. Thus, the f_l's can be factorized into :

$$f_l^{(A)}(\boldsymbol{r}_-, z) = \frac{1}{\sqrt{S}} \exp(i\boldsymbol{k}_- \cdot \boldsymbol{r}_-)\, \chi_l^{(A)}(z) \tag{6}$$

$$f_l^{(B)}(\boldsymbol{r}_-, z) = \frac{1}{\sqrt{S}} \exp(i\boldsymbol{k}_- \cdot \boldsymbol{r}_-)\, \chi_l^{(B)}(z) \tag{7}$$

or in short :

$$f_l^{(A,B)}(\boldsymbol{r}_-, z) = \frac{1}{\sqrt{S}} \exp(i\boldsymbol{k}_- \cdot \boldsymbol{r}_-)\, \chi_l^{(A,B)}(z) \tag{8}$$

where S is the sample area and $\boldsymbol{k}_- = (k_x, k_y)$ is a bi-dimensional wavevector which is the same in the A and B layers in order to comply with the in-plane translational invariance.

Although $\boldsymbol{k}_-$ could theoretically span the whole in-plane section of the hosts' Brillouin zone, it is in practice seldom larger than ~ 1/10 of its size.

We shall denote by $\varepsilon_{l0}^{(A)}$, $\varepsilon_{l0}^{(B)}$ the energies of the l^{th} band edge at the zone centre of the A and B materials respectively. We shall also assume that for all l $\chi_l^{(A,B)}(z)$ varies slowly at the scale of the hosts' unit cell.

Thus, the heterostructure wavefunction $\psi(\boldsymbol{r})$ is a sum of the products of rapidly varying functions : the $u_{l,0}$'s, which are periodic with the hosts' periodicity by slowly varying *envelope functions* : the f_l's.

To lighten the notations, we write the heterostructure Hamiltonian in the form

$$H = \frac{p^2}{2m_0} + V_A(\boldsymbol{r})\, Y_A + V_B(\boldsymbol{r})\, Y_B, \tag{9}$$

where Y_A (Y_B) are step functions which are unity if $\boldsymbol{r}$ corresponds to an A layer (to a B layer). We have

$$Hu_{l0}(\boldsymbol{r}) = (\varepsilon_{l0}^{(A)} Y_A + \varepsilon_{l0}^{(B)} Y_B)\, u_{l0}(\boldsymbol{r}). \tag{10}$$

We now let H act upon $\psi(\boldsymbol{r})$, multiply by $u_{m0}^*(\boldsymbol{r}) \exp(-i\boldsymbol{k}_- \cdot \boldsymbol{r}_-)\, \chi_m^{*(A,B)}(z)$ and integrate over space. Following the same procedure as in Appendix B of chapter II we find that $\chi_l^{(A,B)}(z)$ must fulfil the set of eigenvalue equations :

$$Q^{(0)}\left(z, -i\hbar \frac{\partial}{\partial z}\right) \boldsymbol{\chi} = \varepsilon\, \boldsymbol{\chi}. \tag{11}$$

In equation (11) $\boldsymbol{\chi}$ is a N dimensional column vector and Q a $N \times N$ matrix, where N is the number of bands edges which are retained in equations (1, 2). The $Q^{(0)}$ matrix elements $D_{lm}^{(0)}$ are functions of z and $\partial/\partial z$:

$$D_{lm}^{(0)}\left(z, \frac{\partial}{\partial z}\right) = \left[\varepsilon_{l,0}^{(A)} Y_A + \varepsilon_{l,0}^{(B)} Y_B - \frac{\hbar^2 k_-^2}{2m_0} - \frac{\hbar^2}{2m_0} \frac{\partial^2}{\partial z^2}\right] \delta_{l,m} -$$

$$\frac{\hbar \boldsymbol{k}_-}{m_0} \cdot \langle l | \boldsymbol{p}_- | m \rangle - \frac{i\hbar}{m_0} \langle l | p_z | m \rangle \frac{\partial}{\partial z} \tag{12}$$

where :

$$\langle l | \boldsymbol{p} | m \rangle = \int_{\Omega_m} u_{l0}^{*} \, \boldsymbol{p} u_{m0} \, \mathrm{d}^3 r \tag{13}$$

and Ω_m is the unit cell of the host layers.

By comparing equations (12, 13) with the results obtained in chapter II, we see that $Q^{(0)}$ is nothing but the $\boldsymbol{k}.\boldsymbol{p}$ matrix of bulk materials, except that

i) k_z is replaced by $-i\,\partial/\partial z$

ii) the band edges ε_{l0} are now position-dependent and vary in a steplike manner.

Instead of using $\varepsilon_{l0}^{(A)}$, $\varepsilon_{l0}^{(B)}$ we may denote by V_l the algebraic energy shift of the l^{th} band edge when going from the A to the B material and define the step functions $V_l(z)$ by

$$V_l(z) = 0 \qquad \text{if } z \text{ corresponds to an A layer} \tag{14}$$

$$V_l(z) = \varepsilon_{l0}^{(B)} - \varepsilon_{l0}^{(A)} \qquad \text{if } z \text{ corresponds to a B layer} \tag{15}$$

In the case where an external potential $\varphi(z)$ slowly varying at the scale of the host unit cell is superimposed on the heterostructure potential (e.g. a band bending potential arising from charges), equation (10) is modified by the adjunction of a term $\varphi(z)\,\underset{\sim}{1}$, where $\underset{\sim}{1}$ is the $N \times N$ identity matrix. Similarly, if the external potential is a slowly varying function of $\boldsymbol{r}$, equation (10) should be rewritten as

$$\left[Q^{(0)}\left(\boldsymbol{r}, \frac{\partial}{\partial \boldsymbol{r}} \right) + \varphi(\boldsymbol{r})\,\underset{\sim}{1} \right] \boldsymbol{f} = \varepsilon \boldsymbol{f}, \tag{16}$$

where :

$$D_{lm}^{(0)}\left(\boldsymbol{r}, \frac{\partial}{\partial \boldsymbol{r}} \right) = \left[\varepsilon_{l0}^{(A)} + V_l(z) - \frac{\hbar^2}{2m_0} \left(\frac{\partial^2}{\partial x^2} + \frac{\partial^2}{\partial y^2} + \frac{\partial^2}{\partial z^2} \right) \right] \delta_{lm} - \frac{i\hbar}{m_0} \langle l | \boldsymbol{p} | m \rangle \cdot \frac{\partial}{\partial \boldsymbol{r}} \tag{17}$$

In equation (11) the larger N, the more accurate the results will be (granted that the underlying assumptions of this equation are well justified). In practice, we shall restrict N to 8, i.e. we shall study the heterostructure states which are attached to the Γ_6, Γ_8, Γ_7 bands of the host materials. To the extent that the other host's bands are far from the Γ_6, Γ_8, Γ_7 edges, their effect on the related envelope functions can either be neglected or taken into account only up to the second order in $\boldsymbol{p}$. In the latter case this amounts to replacing the matrix $Q^{(0)}$ in equation (11) by the effective Q given by :

$$Q = Q^{(0)} - \frac{\hbar^2}{2} \sum_{\alpha,\beta} \frac{\partial}{\partial r_\alpha} \underset{\sim}{M}^{\alpha\beta} \frac{\partial}{\partial r_\beta} \tag{18}$$

where $\alpha, \beta = x, y, z$ and $\underset{\sim}{M}^{\alpha\beta}$ is a 8×8 matrix whose coefficients express the indirect Γ_6, Γ_8, Γ_7 couplings *via* a single excursion outside the Γ_6, Γ_8, Γ_7 multiplet (see

Appendix A of the previous chapter) :

$$\frac{m_0}{M_{lm}^{\alpha\beta}} = \frac{2}{m_0} \sum_{\nu} \langle l | p_\alpha | \nu \rangle \frac{1}{\bar{\varepsilon} - \varepsilon_{\nu 0}^{(A)} - V_\nu(z)} \langle l | p_\beta | \nu \rangle \tag{19}$$

where ν labels the remote Γ edges of the host layers, whose energies are position-dependent in the heterostructure (as expressed by the piecewise constant functions $V_\nu(z)$) and where $\bar{\varepsilon}$ in an average energy of the Γ_6, Γ_7, Γ_8 set in the heterostructure.

To summarize, the $\chi_l(z)$ envelope functions are the solutions of a 8×8 second order differential system :

$$\sum_m \left\{ \left[\varepsilon_{m0}^{(A)} - V_m(z) - \frac{\hbar^2 k_\perp^2}{2m_0} - \frac{\hbar^2}{2m_0} \frac{\partial^2}{\partial z^2} \right] \delta_{lm} - \frac{i\hbar}{m_0} \langle l | p_z | m \rangle \frac{\partial}{\partial z} - \right.$$

$$- \frac{\hbar \boldsymbol{k}_\perp}{m_0} \cdot \langle l | \boldsymbol{p}_\perp | m \rangle - \frac{\hbar^2}{2} \frac{\partial}{\partial z} \frac{1}{M_{lm}^{zz}} \frac{\partial}{\partial z} - \frac{i\hbar^2}{2} \sum_\alpha \left[k_\alpha \frac{1}{M_{lm}^{\alpha z}} \frac{\partial}{\partial z} + \frac{\partial}{\partial z} \frac{1}{M_{lm}^{z\alpha}} k_\alpha \right] +$$

$$\left. + \frac{\hbar^2}{2} \sum_{\alpha,\beta} k_\alpha \frac{1}{M_{lm}^{\alpha\beta}} k_\beta \right\} \chi_m = \varepsilon \chi_l \; ; \qquad 1 \leq l \leq 8 \, . \tag{20}$$

As can be seen from equation (20) the problem of the heterostructure energy levels has been reduced to the solution of a set of second order differential equations which govern the spatial behaviour of the slowly varying envelope functions. The microscopic details of the heterostructures, i.e. all the parameters which depend on the rapidly varying phenomena at the scale of the hosts' unit cells, have *explicitly* disappeared from the equations of motion. In equation (20) they only survive through *effective* parameters : the interband matrix elements $\langle l | \boldsymbol{p} | m \rangle$, the effective-mass tensor $M_{lm}^{\alpha\beta}$ and the band offsets V_l. Either these parameters are *a priori* known and equation (20) enables the heterostructure energy levels to be determined, or the band offsets V_l are unknown (as is often the case) and, by comparing the measurements and the energy levels deduced from equation (20), the V_l's being treated as adjustable parameters, these band offsets can be determined. First principle or semi-empirical calculations of the band offsets are available [see e.g. 17-19] and for a given A-B pair the V_l's are determined. In particular, the common anion rule derived by Harrison [17], states that two semiconductors which have a common anion (e.g. GaAs, AlAs), the same crystallographic structure and are lattice matched should nearly have a zero valence band (V_p) offset. This rule however is accurate only up to several tenths of an eV, as any other first principle determination of the V_l's. This is *insufficient* for most practical purposes and one is forced to consider the V_l's as adjustable parameters.

Knowledge of the V_l's is of paramount importance in the heterostructures, as the band offsets decisively influence their energy levels and therefore their electronic properties (see Fig. 3 for an illustration). One of the first tasks when dealing with a given heterostructure is to design experiments which would enable the V_l's to be determined. The reader is referred to [20, 21] for a thorough discussion of the GaAs-AlAs band offsets.

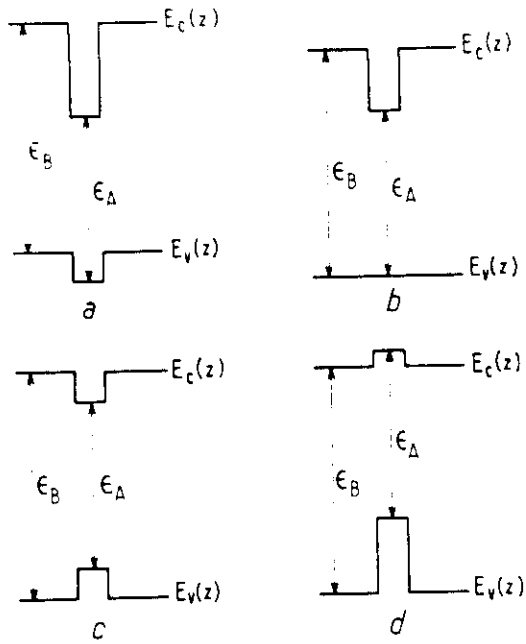

Fig. 3. — Illustration of the part played by different apportionments between the valence and conduction bands of the bandgap energy differences $\varepsilon_B - \varepsilon_A$ of two semiconductors A and B on the electronic states of a BAB rectangular quantum well a) electrons are confined in the A layer, holes in the B layer (type II quantum well) ; b) same as a) except that the A layer is no longer a barrier for holes ; c) both electrons and holes are essentially confined in the A layer (type I quantum well) ; d) the A layer is a barrier for electrons and a well for holes. This structure is thus a type II quantum well, inverted with respect to a). Out of these four structures only c) will display significant excitonic absorption, photoluminescence and stimulated emission. Structure c) is a good candidate for low threshold lasing action.

At the hetero-interface $z = z_0$ we saw that χ is continuous. If we now integrate equation (20) across the interface, we obtain a second set of boundary conditions. These can be cast in the form :

$$\underset{\sim}{A}^{(A)} \chi^{(A)}(z = z_0) = \underset{\sim}{A}^{(B)} \chi^{(B)}(z = z_0) \tag{21}$$

where $\underset{\sim}{A}$ is a 8×8 matrix whose elements are, at most, of the first order in $\frac{\partial}{\partial z}$:

$$A_{lm} = \frac{-\hbar^2}{2m_0} \left| \left(\delta_{lm} + \frac{m_0}{M_l^{zz}} \right) \frac{\partial}{\partial z} + \frac{2i}{\hbar} \langle l | p_z | m \rangle + i \sum_{\alpha = x, y} \frac{m_0}{M_{lm}^{z\alpha}} k_\alpha \right| \tag{22}$$

where we have made use [22-24] of the property

$$M_{lm}^{zz} = M_l^{zz} \delta_{lm}. \tag{23}$$

It is worth pointing out that A_{lm} is *not* diagonal in (l, m) and, *a fortiori*, does not reduce to $\frac{-\hbar^2}{2m_0}\delta_{lm}\frac{\partial}{\partial z}$. Although familiar, the continuity condition of $\frac{d\chi}{dz}$ is only valid in very special circumstances. In fact it is the limit of equation (22) in the empty lattice approximation, where all the u_{l0}'s and u_{a0}'s are constant, which leads to vanishing $(M^{\alpha\beta}_{lm})^{-1}$ and $\langle l|p_z|m\rangle$. We show in Appendix A that equation (22), when applied to a heterostructure whose host layers are both characterized by non degenerate parabolic and isotropic bands but by different effective masses (Ben Daniel-Duke model [25]), is compatible with the conservation of the probability current across the heterostructure and thus with the stationarity of the heterostructure state. On the other hand, the continuity condition of $\frac{d\chi}{dz}$ is incompatible with these conservation laws and should therefore be rejected.

In the following we shall apply the envelope function machinery to various examples. We shall deal either with single quantum wells or with superlattices. The latter heterostructures are obtained by infinitely repeating a sequence of two adjacent A and B layers. The A(B) thickness will be denoted by $L_A(L_B)$ and the superlattice period by d ($d = L_A + L_B$). The growth axis will be taken along the z direction and the first Brillouin zone of the superlattice will correspond to the superlattice wavevector q such that

$$\frac{\pi}{d} < q \leqslant + \frac{\pi}{d} \tag{24}$$

Although equations [5, 21, 22] tell us how to match χ and $\frac{1}{A}\chi$ across the interfaces, we need to know the asymptotic behaviour of χ at large z to complete the determination of the eigensolutions. This asymptotic behaviour depends on the heterostructure under consideration. For superlattices, the band edge profile is periodic upon z with a periodicity d. Thus χ is a Bloch wave

$$\chi(z - d) = \exp(iqd)\,\chi(z) \tag{25}$$

For the bound states of a quantum well, χ should tend to zero at large $|z|$:

$$\lim_{z \to \infty} \chi(z) = 0\,. \tag{26}$$

We shall first discuss the Ben Daniel-Duke model, then the $\mathbf{k}_\perp = \mathbf{0}$ quantum well levels and the superlattice dispersion relations of heterostructures whose host energy levels are well described by the Kane model. The in-plane dispersion relations will finally be considered in section III.

II.3 THE BEN DANIEL-DUKE MODEL. — This model of heterostructure energy levels is the simplest one and works qualitatively for the lowest conduction states of GaAs-Ga(Al)As heterostructures with GaAs layer thickness larger than ~ 100 Å and for the heavy hole levels at $\mathbf{k}_\perp = \mathbf{0}$ in any heterostructure. It amounts to assuming that the heterostructure envelope function is built from host quantum states which

belong to a single parabolic band. For simplicity we shall take an isotropic band and, for definiteness, a conduction band. The effective masses in the A(B) layers will be denoted by $m_A(m_B)$. Each of the levels is twice degenerate (Kramers degeneracy). Equation (20) simplifies considerably as all the host bands are remote to the conduction edge under consideration. Thus, we can write

$$\left[\varepsilon_s + V_s(z) - \frac{\hbar^2}{2} \frac{\partial}{\partial z} \frac{1}{\mu(z)} \frac{\partial}{\partial z} + \frac{\hbar^2 k_\perp^2}{2\mu(z)} \right] \chi(z) = \varepsilon \chi(z) \tag{27}$$

$$\mu^{-1}(z) = m_0^{-1} + (M_{cc}^{zz})^{-1} \tag{28}$$

$$\mu(z) = \begin{cases} m_A & \text{if} \quad z \text{ corresponds to an A layer} \\ m_B & \text{if} \quad z \text{ corresponds to a B layer} \end{cases} \tag{29}$$

$$V_s(z) = \begin{cases} 0 & \text{if} \quad z \text{ corresponds to an A layer} \\ V_s & \text{if} \quad z \text{ corresponds to a B layer} \end{cases} \tag{30}$$

and V_s is the algebraic energy shift of the S band edge when going from the A to the B material. The boundary conditions at the A-B interfaces are also very simple. They are such that :

$$\chi(z) \qquad \text{and} \qquad \frac{1}{\mu(z)} \frac{d\chi}{dz} \tag{31}$$

are both continuous. It should be noticed that the effective mass mismatch contributes to the total confining barrier by a term which is $k_\perp$-dependent and, like $V_s(z)$, exhibits step-like variations. This extra term is however small in most instances (e.g. conduction states in GaAs-$Ga_{1-x}Al_xAs$, $Ga_{0.47}In_{0.53}As$-InP quantum wells) although it leads to a decreasing effective barrier height with increasing $k_\perp$ if $m_B > m_A > 0$.

It is also interesting to notice that the effective mass mismatch leads to a *discontinuity in the derivative* of the envelope function at the interfaces. In the extreme case where m_A and m_B are of opposite signs, this discontinuity causes a cusp at the interfaces of the envelope function. The latter situation occurs in HgTe-CdTe heterostructures (but only at $\boldsymbol{k}_\perp = \mathbf{0}$) (see section II 3.2).

II.3.1 *The Ben Daniel-Duke quantum wells* ($m_A m_B > 0$). — The $k_\perp$-dependent potential energy $V_s(z) + \dfrac{\hbar^2 k_\perp^2}{2\mu(z)}$ is even with respect to the middle of the A layer. Thus, as in chapter I, one can look for bound states solutions in the following forms

$$\begin{aligned} \chi_{even}(z) &= A \cos(k_A z) && |z| \leqslant \frac{L_A}{2} \\ \chi_{even}(z) &= B \exp\left[-\kappa_B \left(z - \frac{L_A}{2} \right) \right] && z \geqslant \frac{L_A}{2} \\ \chi_{even}(-z) &= \chi_{even}(z) \end{aligned} \tag{32}$$

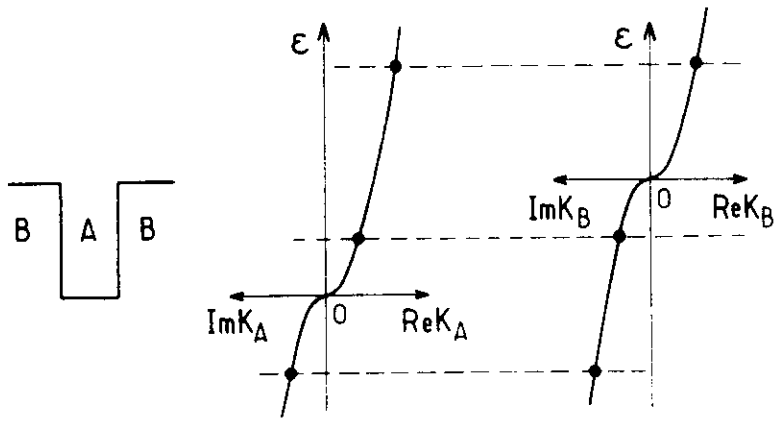

Fig. 4. — Dispersion relations *versus* the real and imaginary wavevectors in the A and B layers stacked to form a BAB quantum wells. The three dashed lines, drawn for three energies in the heterostructures and for $k_{\parallel} = 0$, show which wavevectors in each kind of layers participate in the heterostructure state. The upper line corresponds to a delocalized quantum well state and the middle line to a quantum well bound state. No heterostructure state can be associated with the lower line as the carrier effective masses are assumed to have the same sign in this particular Ben Daniel-Duke quantum well.

or :

$$\begin{aligned} \chi_{odd}(z) &= A \sin(k_A z) && |z| \leq \frac{L_A}{2} \\ \chi_{odd}(z) &= B \exp\left[-\kappa_B\left(z - \frac{L_A}{2}\right)\right] && z \geq \frac{L_A}{2} \\ \chi_{odd}(-z) &= -\chi_{odd}(z) \end{aligned} \tag{33}$$

with :

$$\varepsilon - \varepsilon_v = \frac{\hbar^2 k_A^2}{2m_A} + \frac{\hbar^2 k_{\parallel}^2}{2m_A} = V_v - \frac{\hbar^2 \kappa_B^2}{2m_B} + \frac{\hbar^2 k_{\parallel}^2}{2m_B}. \tag{34}$$

Equations (32-34) hold if $\kappa_B^2 > 0$, i.e. if the heterostructure state is built from the evanescent states of the B layers (see Fig. 4).

By matching $\chi(z)$ and $\mu^{-1}(z)\frac{d\chi}{dz}$ at the interface $z = \frac{L_A}{2}$ (or equivalently $z = -\frac{L_A}{2}$), one obtains the implicit equations whose roots are the bound solutions of the Ben Daniel-Duke quantum well problem. These are :

$$\cos\varphi_A - \frac{m_B}{m_A}\frac{k_A}{\kappa_B}\sin\varphi_A = 0 \qquad \text{for even states} \tag{35}$$

$$\cos \varphi_A + \frac{m_A}{m_B} \frac{\kappa_B}{k_A} \sin \varphi_A = 0 \qquad \text{for odd states} \tag{36}$$

$$\varphi_A = \frac{1}{2} k_A L_A \tag{37}$$

A comparison with the results obtained in chapter I shows that equations (35-37) are the same as those of text book quantum wells except that the wavevectors k_A, κ_B have been replaced by k_A/m_A and κ_B/m_B. This is a direct consequence of the matching conditions of $\mu^{-1}(z) \frac{d\chi}{dz}$ at the interfaces. In all other instances however, many of the results obtained in chapter I can be applied to equations (35-37). In particular, the number of states bound by the well (at $k_{\perp} = 0$) is equal to

$$N = 1 + \text{Int} \left[\left(\frac{2m_A}{\hbar^2 \pi^2} V_s L_A^2 \right)^{1/2} \right] \tag{38}$$

In figure 5 are shown the variations of the confinement energies E_1, E_2, E_3 at $\boldsymbol{k}_{\perp} = \boldsymbol{0}$ of a Ben Daniel-Duke quantum well ($L_A = 100$ Å, $V_s = 0.3$ eV

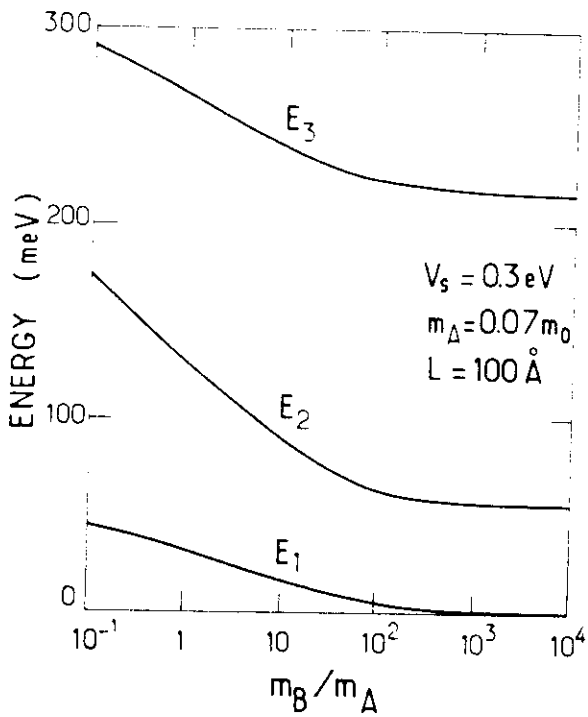

Fig. 5. — Evolution of the confinement energies E_1, E_2, E_3 with the mass ratio $\frac{m_B}{m_A}$ in a B Daniel-Duke quantum well. $L = 100$ Å ; $V_s = 0.3$ eV; $m_A = 0.07\, m_0$.

$m_A = 0.07\ m_0$) with the mass ratio $\frac{m_B}{m_A}$. It can be seen that all the E_i's decrease with increasing $\frac{m_B}{m_A}$ and tend to values E_{p+1}^{∞} which are such that :

$$k_A\,(E_{p+1}^{\infty})\,L_A = p\pi \qquad p = 0, 1, 2\ldots \tag{39}$$

This equation resembles the bound states equation in a quantum well with an infinite barrier height. It expresses however quite a different physical situation. In a quantum well with infinite V_0, the envelope function vanishes at the interface. Besides, according to equation (38), V_0 is infinite. If V_0 diverges, κ_B also diverges. This leads either to $\cos \varphi_A = 0$ (Eq. (35)) or $\sin \varphi_A = 0$ (Eq. (36)). The ground state solution, which is nodeless, fulfils $L_A k_A(V_0 = \infty) = \pi$, the associated envelope function having a finite slope at $z = \pm \frac{L_A}{2}$. On the other hand, when V_0 is kept fixed but m_B/m_A increases to infinity, V_0 remains unchanged. Moreover, if the ground states envelope function is to be nodeless, it has to be a cosine in the well. It should barely penetrate the barrier (since κ_B increases) and, in addition, should have a derivative at $z = \pm \frac{L_A}{2}$ whose modulus becomes smaller and smaller to comply with the continuity of $\mu^{-1}(z)\frac{d\chi}{dz}$ at the interface. Thus at infinite m_B/m_A ratio the only possible wave function is constant in the well and zero in the barrier, so that both the envelope function and its derivative are also zero in the barrier. The only $\cos(k_A z)$ function which is constant corresponds to $k_A = 0$ and thus to $E_1 = 0$... This is why when m_B/m_A diverges and V_0 is fixed the even states of the well fulfil $\sin \varphi_A = 0$ (and not $\cos \varphi_A = 0$), i.e. admit $E_1 = 0$ as an acceptable solution.

Symmetrically, the odd states fulfil $\cos \varphi_A = 0$ and finally the series of levels (Eq. (39)) is recovered. The ground state envelope function of a quantum well with either infinite V_0 or finite V_0 but infinite m_B is shown in figure 6 in order to depict the differences between the two physical situations.

When the effective masses m_A and m_B are not widely different, as for instance in GaAs-Ga(Al)As heterostructures, the in-plane dispersions of the subbands attached to the $\boldsymbol{k}_{\perp} = \mathbf{0}$ bound states of a quantum well are nearly parabolic in $k_{\perp}$:

$$E_n(k_{\perp}) \simeq \varepsilon_0 + E_n(0) + \frac{\hbar^2 k_{\perp}^2}{2m_n} \tag{40}$$

The in-plane mass m_n should, in principle, be obtained by numerically solving equations (32-37). However when $k_{\perp}$ is small enough, an approximate scheme can be designed in the following way. The term $\hbar^2 k_{\perp}^2/2\mu(z)$ in equation (27) is formally rewritten :

$$\frac{\hbar^2 k_{\perp}^2}{2\mu(z)} = \frac{\hbar^2 k_{\perp}^2}{2m_n} + \frac{\hbar^2 k_{\perp}^2}{2}\left[\frac{1}{\mu(z)} - \frac{1}{m_n}\right] \tag{41}$$

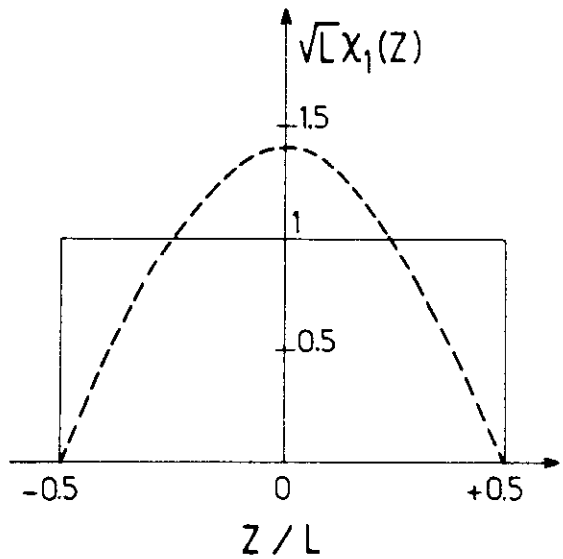

Fig. 6. — Ground state envelope functions for a quantum well with infinite V_0 (dashed line) or for a quantum well with finite V_0 but infinite $\frac{m_b}{m_a}$ (solid line).

and the second term on the right-hand side of equation (41) is considered as a perturbation to $\mathscr{H}_0$ where

$$\mathscr{H}_0 = \varepsilon_n + V_0(z) = \frac{\hbar^2}{2}\frac{\partial}{\partial z}\frac{1}{\mu(z)}\frac{\partial}{\partial z} + \frac{\hbar^2 k_\perp^2}{2m_n}, \tag{42}$$

whose eigenstates are in the form given by equation (40). The first order corrections to these eigenstates are given by :

$$\Delta E_n = \frac{\hbar^2 k_\perp^2}{2}\left[\frac{1}{m_A}\left[1 - P_b(E_n)\right] + \frac{1}{m_B}P_b(E_n) - \frac{1}{m_n}\right] \tag{43}$$

where :

$$P_b(E_n) = 2\int_{\frac{L_A}{2}}^{\frac{L}{2}} \chi_n^2(z)\,dz = \frac{B^2}{\kappa_B} \tag{44}$$

is the integrated probability of finding the electron in the barriers while in the E_n state. The first order energy shift will vanish if :

$$\frac{1}{m_n} = \frac{1}{m_A}\left[1 - P_b(E_n)\right] + \frac{1}{m_B}P_b(E_n). \tag{45}$$

Equation (45) defines the in-plane effective mass of the n^{th} subband in the vicinity of $k_{\perp} = 0$. It may be remarked that if $m_B \gg m_A$, as is the case in GaAs-Ga(Al)As or $Ga_{0.4}$-$In_{0.53}$As-InP, this in-plane mass m_n will increase with increasing subband index n.

Using the approximately parabolic in-plane dispersion laws (equation (40)) it is very easy to calculate the density of states $\rho(\varepsilon)$ associated with the bound states E_n. Proceeding exactly as in chapter I we obtain :

$$\rho(\varepsilon) = \sum_n \rho_n(\varepsilon) \tag{46a}$$

$$\rho_n(\varepsilon) = \frac{m_n S}{\pi \hbar^2} Y(\varepsilon - E_n) \tag{46b}$$

where $Y(x)$ is the step function. We recover the familiar staircase density of states. The properties of a Ben Daniel-Duke quantum well are summarized in figure 7.

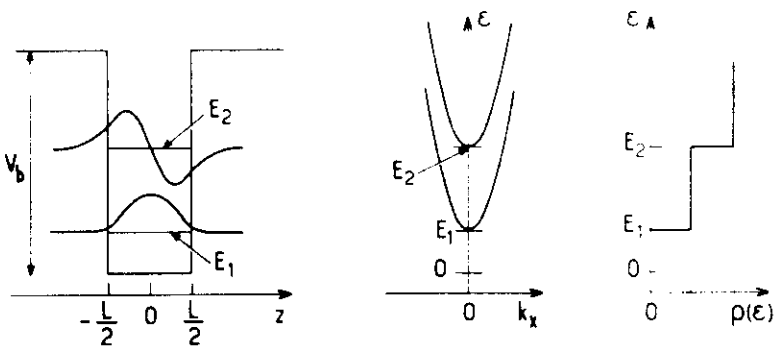

Fig. 7. — A recollection of the main properties of the quantum well bound states, solutions of a Ben Daniel-Duke Hamiltonian. From left to right : conduction band edge profile, energy levels E_1 and E_2 and their associated envelope functions ; in-plane dispersion relations of the E_1 and E_2 subbands ; energy dependence of the heterostructure density of states $\rho(\varepsilon)$.

II.3.2 *Interface states of Ben Daniel-Duke quantum wells* ($m_A m_B < 0$; $\boldsymbol{k}_{\perp} = \mathbf{0}$). — The case $m_A m_B < 0$ is practically realized in HgTe-CdTe heterostructures [26] (see Fig. 8). CdTe is a conventional open gap semiconductor whose level ordering is the same as is found in GaAs. HgTe is a symmetry-induced zero gap semiconductor. The Γ_6 band, which is a conduction band in most III-V and II-VI semiconductors, is a light hole band in HgTe. The Γ_6 edge lies ~ 0.3 eV below the Γ_8 edges. As the Γ_8 light band and Γ_6 band are nearly mirror-like, the Γ_8 light band is a conduction band in HgTe, degenerate at the zone centre with the Γ_8 heavy hole band (inversion asymmetry splitting having been neglected).

Ignoring the absence of centro-symmetry of the zinc-blende lattice, we shall see in section (II.4) that the light particle and heavy hole states decouple at $\boldsymbol{k}_{\perp} = \mathbf{0}$. We can

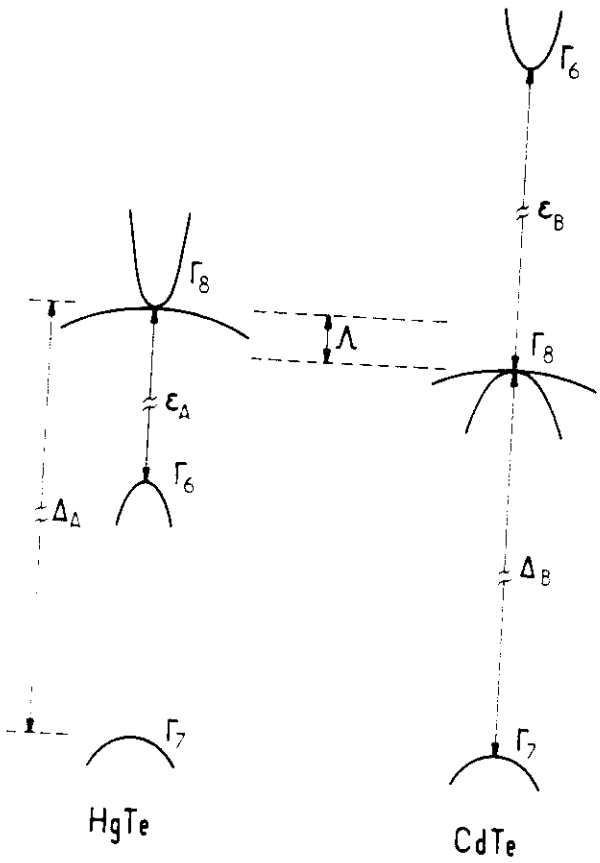

Fig. 8. — Band structures of bulk HgTe (left panel) and CdTe (right panel) in the vicinity of the Γ point (schematic).

thus treat the problem of the light particle states associated with a Γ_8 edge as if we were considering a single band. The interesting feature of the HgTe-CdTe heterostructure is that the light particle changes the sign of its effective mass across the interfaces, being electron-like in the HgTe layer and light hole-like in the CdTe layers. To be specific, let us consider a CdTe-HgTe-CdTe double heterostructure.

According to [27] the bottom of the HgTe Γ_8 conduction band lies at an energy .1 ~ 40 meV above the top of the CdTe Γ_8 valence band. Thus, bound states of the heterostructure only exist if $\varepsilon \geq -.1$ (the energy zero being taken at the Γ_8 edge in HgTe). If $-.1 \leq \varepsilon \leq 0$, the states are evanescent in both kinds of layers while if $\varepsilon \geq 0$, the carrier wavevector is real (imaginary) in the HgTe (CdTe) layers. Clearly, bound states of positive energies will exist (an infinite number in the one-band description of each host layer). Proceeding as in section II 3.1 their energies will

fulfil

$$\cos \varphi_A + \frac{|m_B|}{m_A} \frac{k_A}{\kappa_B} \sin \varphi_A = 0 \qquad \text{for even states} \tag{47}$$

$$\cos \varphi_A - \frac{m_A}{|m_B|} \frac{\kappa_B}{k_A} \sin \varphi_A = 0 \qquad \text{for odd states} \tag{48}$$

$$\varphi_A = \frac{1}{2} k_A L_A \tag{49}$$

$$k_A = \sqrt{\frac{2m_A}{\hbar^2} \varepsilon} \; ; \qquad \kappa_B = \sqrt{\frac{2|m_B|}{\hbar^2} (\varepsilon + A)} \tag{50}$$

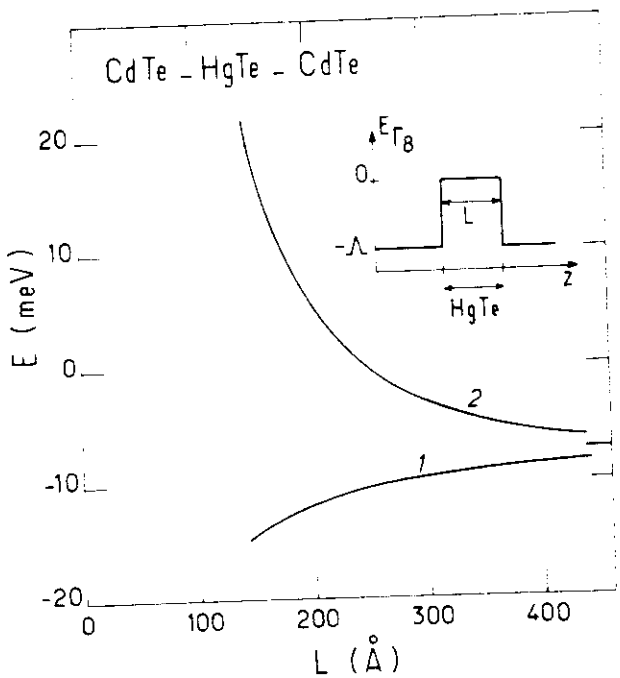

Fig. 9. — Evolution of the ground and first excited bound states (labelled 1 and 2 respectively) *versus* the HgTe slab thickness in a CdTe-HgTe-CdTe double heterostructure.

The bound state wavefunctions are all characterized by *cusps* at the interfaces due to the change in the carrier effective mass at the hetero-interfaces. This sign reversal also implies that equation (48) can be fulfilled at $\varepsilon = 0$ for a certain L_A while equation (47) can not. This means that at least one state (even in z) should lie below the bottom of the HgTe conduction band edge. This state is an interface level, built from evanescent states in *each* of the host layers, whose wavefunction peaks at the

interface. More precisely, we can write :

$$\chi_1(z) = A\cosh(\kappa_A z) \qquad |z| \leqslant \frac{1}{2} L_A \tag{51}$$

$$\chi_2(z) = B\exp\left[-\kappa_B\left(z - \frac{1}{2}L_A\right)\right] \qquad z \geqslant \frac{1}{2} L_A \tag{52}$$

$$\chi_2(-z) = \chi_2(z) \tag{53}$$

with : $$\kappa_A = \sqrt{\frac{2m_A}{\hbar^2}(\varepsilon - \varepsilon)}; \qquad \kappa_B = \sqrt{\frac{2|m_B|}{\hbar^2}(\varepsilon - V)}. \tag{54}$$

By matching $\chi_1(z)$ and $\mu^{-1}(z)\dfrac{d\chi_1}{dz}$ at $z = \dfrac{1}{2}L_A$, we find that ε should be the root of the implicit equation

$$\tanh\left(\frac{1}{2}\kappa_A L_A\right) = \frac{m_A}{|m_B|}\frac{\kappa_B}{\kappa_A} \tag{55}$$

It is very easy to check that equation (55) always admits one solution E_1 (and only one) which extrapolates to $-V$ when $L_A \to 0$. A second state may actually exist in the energy segment $[-V, 0]$ if the HgTe layer is thick enough. It corresponds to an odd envelope function :

$$\chi_1(z) = A\sinh(\kappa_A z) \qquad |z| \leqslant \frac{1}{2} L_A \tag{56}$$

$$\chi_2(z) = B\exp\left[-\kappa_B\left(z - \frac{1}{2}L_A\right)\right]; \qquad z \geqslant \frac{1}{2} L_A \tag{57}$$

$$\chi_2(-z) = -\chi_2(z) \tag{58}$$

The E_2 energy is the solution of the implicit equation :

$$\coth\left(\frac{1}{2}\kappa_A L_A\right) = \frac{m_A}{|m_B|}\frac{\kappa_B}{\kappa_A} \tag{59}$$

which admits a solution if

$$L_A > \frac{2|m_B|}{m_A}\sqrt{\frac{\hbar^2}{2|m_B|V}} \tag{60}$$

Again, the solution of equation (59), if it exists, is unique. When L_A becomes very large the energies E_1 and E_2 converge to the value :

$$E_\infty = -\frac{V}{1 + \dfrac{|m_B|}{m_A}} \tag{61}$$

which is the energy position of the interface state in a single HgTe-CdTe heterojunction [28, 29]. Clearly, at large L_A (i.e. $\kappa_A L_A \gg 1$) the two states E_1 and E_2 are very well approximated by the symmetric and antisymmetric combinations of the two interface states centred at $\pm\dfrac{1}{2}L_A$ respectively. The

behaviour of E_1 and E_2 *versus* L_A is presented in figure 9 to illustrate the previous discussion. In figure 10 we show the calculated $\chi_1(z)$ envelope functions in $Hg_{1-x}Cd_xTe$-HgTe-$Hg_{1-x}Cd_xTe$ quantum wells to illustrate the interface nature of the E_1 state. Although the existence of the interface state relies only on the relative position of the Γ_8 edges of HgTe and CdTe, their actual energy position, as well as their behaviour at $\boldsymbol{k}_\perp \neq \mathbf{0}$ (where they strongly couple to the heavy hole states), remains a subject of active research.

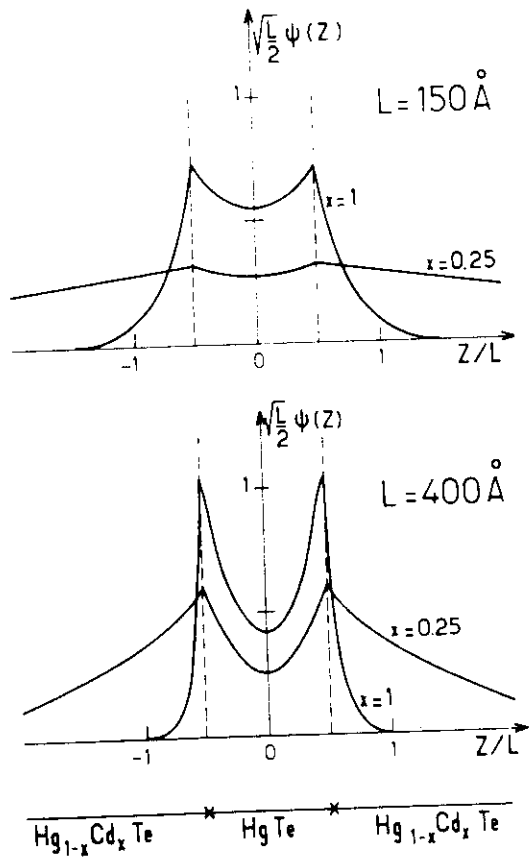

Fig. 10. — Dimensionless envelope functions of the ground states in $Hg_{1-x}Cd_xTe$-HgTe-$Hg_{1-x}Cd_xTe$ double heterostructures ($x = 1$ and $x = 0.2$) for two different HgTe slab thicknesses.

II.4 QUANTUM WELLS AND SUPERLATTICES WITH HOSTS WHICH DISPLAY KANE-LIKE BANDS. — This situation is found in most of the III-V and II-VI heterostructures, e.g. GaAs-Ga(Al)As, $Ga_{0.47}In_{0.53}As$-InP, HgTe-CdTe, $Ga_{0.47}In_{0.53}As$-$Al_{0.48}In_{0.52}As$ etc... At $\boldsymbol{k}_\perp = \mathbf{0}$ the 8×8 differential system defined in equation (20) is block-diagonal if the u_{j0} basis diagonalizes both the total angular momentum

J and its z projection J_z. Specifically we shall take

$$\begin{aligned}
u_{10} &= \left| S, \frac{1}{2}, \frac{1}{2} \right\rangle && |S^{\uparrow}\rangle \\
u_{30} &= \left| P, \frac{3}{2}, \frac{3}{2} \right\rangle && = \frac{1}{\sqrt{2}} |(X+iY)^{\uparrow}\rangle \\
u_{50} &= \left| P, \frac{3}{2}, \frac{1}{2} \right\rangle && = \sqrt{\frac{2}{3}} |Z^{\uparrow}\rangle + \frac{1}{\sqrt{6}} |(X+iY)^{\downarrow}\rangle \\
u_{70} &= \left| P, \frac{1}{2}, \frac{1}{2} \right\rangle && = \frac{1}{\sqrt{3}} |(X+iY)^{\downarrow}\rangle + \frac{1}{\sqrt{3}} |Z^{\uparrow}\rangle \\
u_{20} &= \left| S, \frac{1}{2}, -\frac{1}{2} \right\rangle && = |S^{\downarrow}\rangle \\
u_{40} &= \left| P, \frac{3}{2}, -\frac{3}{2} \right\rangle && = \frac{1}{\sqrt{2}} |(X-iY)^{\downarrow}\rangle \\
u_{60} &= \left| P, \frac{3}{2}, -\frac{1}{2} \right\rangle && = \frac{1}{\sqrt{6}} |(X-iY)^{\uparrow}\rangle - \sqrt{\frac{2}{3}} |Z^{\downarrow}\rangle \\
u_{80} &= \left| P, \frac{1}{2}, -\frac{1}{2} \right\rangle && = \frac{1}{\sqrt{3}} |(X-iY)^{\uparrow}\rangle - \frac{1}{\sqrt{3}} |Z^{\downarrow}\rangle
\end{aligned} \tag{62}$$

The differential system $\underline{D}\boldsymbol{\chi} = \varepsilon\boldsymbol{\chi}$ factorizes into:

$$\begin{bmatrix} \underline{D}_+ & 0 \\ 0 & \underline{D}_- \end{bmatrix} \begin{bmatrix} \boldsymbol{\chi}_+ \\ \boldsymbol{\chi}_- \end{bmatrix} = \varepsilon \begin{bmatrix} \boldsymbol{\chi}_+ \\ \boldsymbol{\chi}_- \end{bmatrix} \tag{63}$$

where $\underline{D}_+$, $\underline{D}_-$, $\boldsymbol{\chi}_+$, $\boldsymbol{\chi}_-$ are 4×4 matrices and 4×1 column vectors respectively. $\underline{D}_+$ and $\underline{D}_-$ are identical and therefore each eigenenergy will be twice degenerate. $\underline{D}_+$ (and $\underline{D}_-$) are equal to:

$D_+\left(z, p_z = -i\hbar\frac{\partial}{\partial z}\right) =$

$V_s(z) + \frac{1}{2m_0} p_z F p_z$	0	$\sqrt{\frac{2}{3}} P p_z$	$\frac{P}{\sqrt{3}} p_z$
0	$-\varepsilon_A + V_p(z)$ $\frac{1}{2m_0} p_z (\gamma_1 - 2\gamma_2) p_z$	0	0
$-\sqrt{\frac{2}{3}} P p_z$	0	$-\varepsilon_A + V_p(z)$ $\frac{1}{2m_0} p_z (\gamma_1 + 2\gamma_2) p_z$	$\frac{\sqrt{2}}{m_0} p_z \gamma_2 p_z$
$\frac{P}{\sqrt{3}} p_z$	0	$\frac{\sqrt{2}}{m_0} p_z \gamma_2 p_z$	$-\varepsilon_A - \Delta_A$ $+ V_s(z) - \frac{1}{2m_0} p_z \gamma_1 p_z$

(64)

where $V_p(z)$ and $V_\delta(z)$ are the step functions which describe the algebraic shifts of the Γ_8 and Γ_7 edges when going from the A to the B materials and :

$$P = \frac{-i}{m_0}\langle S|p_x|X\rangle = \frac{-i}{m_0}\langle S|p_y|Y\rangle = \frac{-i}{m_0}\langle S|p_z|Z\rangle \tag{64a}$$

In equation (64) we have included the free electron term in the definition of F, γ_1, γ_2 :

$$F = \frac{2}{m_0}\sum_{\nu}\langle S|p_x|\nu\rangle\frac{1}{\bar{\varepsilon} - \varepsilon_{\nu 0}^{(A)} - V_\nu(z)}\langle\nu|p_x|S\rangle + 1 \tag{64b}$$

$$\gamma_1 = \frac{-2}{3m_0}\sum_{\nu}\frac{\langle X|p_x|\nu\rangle\langle\nu|p_x|X\rangle + 2\langle X|p_y|\nu\rangle\langle\nu|p_y|X\rangle}{\bar{\varepsilon} - \varepsilon_{\nu 0}^{(A)} - V_\nu(z)} - 1 \tag{64c}$$

$$\gamma_2 = \frac{-1}{3m_0}\sum_{\nu}\frac{\langle X|p_x|\nu\rangle\langle\nu|p_x|X\rangle - \langle X|p_y|\nu\rangle\langle\nu|p_y|X\rangle}{\bar{\varepsilon} - \varepsilon_{\nu 0}^{(A)} - V_\nu(z)} \tag{64d}$$

The explicit z dependences of F, γ_1, γ_2 (*via* the $V_\nu(z)$ functions) has led us to use combinations like $p_z F p_z$, $p_z\,\gamma_1\,p_z$, $p_z\,\gamma_2\,p_z$ in equation (64) to ensure the hermiticity of D_z.

It is important to notice that the $\left|P, \frac{3}{2}, \pm\frac{3}{2}\right\rangle$ lines are uncoupled to the others in equation (64). The associated envelope functions correspond to the heavy hole states which can therefore be treated separately from the other light particle states. The latter are hybrids of Γ_6, Γ_8 light and Γ_7 host states which are admixed by the non-parabolicity of the host materials and the $V_s(z)$, $V_p(z)$, $V_\delta(z)$ functions (see Appendix B of the previous chapter). Notice however that the decoupling between heavy holes and light particles is only approximate as, even at $\mathbf{k}_\parallel = \mathbf{0}$, the effect of the non centro-symmetry of the host zinc blende lattices in equation (64) has been neglected. This effect is usually very small (smaller in III-V than in II-VI compounds) and may eventually be treated in perturbation (see Appendix B). Its main effect is to prevent any crossing between light and heavy particle states. The latter would occur, for instance, in a quantum well when the confinement energy of a heavy hole state HH_n equals that of a light hole state LH_n for certain thicknesses of the well-acting material. Notice that the lack of centro-symmetry appears automatically in tight-binding calculations [6] where the difference between the anion and the cation in the host's unit cell is naturally taken into account.

Across a A-B interface, the boundary conditions are such that χ_ν ($\chi_{\nu'}$) and $\underset{\sim}{A}_\nu\,\chi_\nu$ ($\underset{\sim}{A}_{\nu'}\,\chi_{\nu'}$) are continuous where $\underset{\sim}{A}_\nu$ equals $\underset{\sim}{A}_{\nu'}$ and

$$\underset{\sim}{A}_\nu\left(z, \frac{\partial}{\partial z}\right) = \begin{bmatrix} F\frac{\partial}{\partial z} & 0 & 0 & 0 \\ 0 & -(\gamma_1 - 2\gamma_2)\frac{\partial}{\partial z} & 0 & 0 \\ 0 & 0 & -(\gamma_1 + 2\gamma_2)\frac{\partial}{\partial z} & 2\sqrt{3}\,\gamma_2\frac{\partial}{\partial z} \\ 0 & 0 & 2\sqrt{3}\,\gamma_2\frac{\partial}{\partial z} & -\gamma_1\frac{\partial}{\partial z} \end{bmatrix} \tag{65}$$

where we have made use of the χ_ν continuity to simplify $A_{\nu\nu'}$.

As expected, $\underline{A}_{-}$ only involves *small* terms, which arise either from the free electron contribution or from the $\boldsymbol{k}.\boldsymbol{p}$ interaction between Γ_6, Γ_7, Γ_8 and the remote edges. This interaction is very important for heavy hole states since the heavy hole bands would be dispersionless in the hosts if this interaction was neglected. On the other hand, for light particle states, the F, γ_1, γ_2 parameters contribute very little to the host effective mass. Their presence allows a much better fit of these effective masses than was obtained by retaining only a single parameter (P). In fact, we have to account for four band edge effective masses. With P, F, γ_1 and γ_2 we obtain four adjustable parameters, which is the required number.

The reasons why we wish to discard the remote band parameters for light particle states are twofold. Firstly, without F, γ_1 and γ_2, the differential system for the three light particle components of $\boldsymbol{\chi}_{-}$ becomes of the first order in $\frac{\partial}{\partial z}$ and therefore easier to handle, to the extent that all the results can be obtained in closed forms. Secondly, by retaining F, γ_1 and γ_2, we face a difficulty termed by White and Sham [1] the "wing bands", which are extensively discussed by Schuurman and t'Hooft [3].

Let us try to pinpoint the origins of this difficulty by using a simplified model : we shall neglect the Γ_7 band, i.e. we shall assume that the spin-orbit energy is very large compared with the light hole confinement energy. In each type of layer, the heterostructure states of a given energy ε are linear combinations of bulk solutions. These solutions are either propagating (k_A, k_B real) or evanescent (k_A real, k_B imaginary) in the A and/or B layers. Thus in order to know our heterostructure states, we simply have to calculate the k_A, k_B corresponding to the energy ε. Therefore to calculate k_A, for example, we have to find the roots of :

$$\text{Det}\left[\underline{D}_{-}(p_z \to \hbar k_A) - \varepsilon \underline{1}\right] = 0 \tag{66}$$

In our three band (Γ_{8h}, Γ_{8l}, Γ_6) model, equation (66) factorizes into

$$\left(\varepsilon - \varepsilon_A - \frac{\hbar^2 k_A^2}{2M_{8h}^{[A]}}\right)\left[\left(\varepsilon - \frac{F\hbar^2 k_A^2}{2m_0}\right)\left(\varepsilon - \varepsilon_A + (\gamma_1 - 2\gamma_2)\frac{\hbar^2 k_A^2}{2m_0}\right) - \frac{2\hbar^2}{3}P^2 k_A^2\right] = 0 \tag{67}$$

The first root is obvious and describes the heavy hole branch. At the moment however, it is of no concern to us. The two other k_A^2 roots, which are always real, describe the dispersions of either the *coupled* ($\Gamma_6 - \Gamma_8^l$) bands or the wing band (see Fig. 11). The former, which has a clear physical significance is i) small compared with the size of the A Brillouin zone along the z axis and ii) almost insensitive to any change in the small parameters F and $\gamma_1 - 2\gamma_2$. k_A is real for both $\varepsilon < -\varepsilon_A$ and $\varepsilon > 0$ and imaginary for $-\varepsilon_A \leq \varepsilon \leq 0$: the propagating light hole state ($\varepsilon \leq -\varepsilon_A$) becomes evanescent as ε enters into the bandgap $\left(-\varepsilon_A \leq \varepsilon \leq -\frac{\varepsilon_A}{2}\right)$ and progressively transforms into an evanescent Γ_6 electron $\left(-\frac{\varepsilon_A}{2} \leq \varepsilon \leq 0\right)$, ending up as a propagating electron state ($\varepsilon \geq 0$). The other k_A^2 root is unphysical as i) it has a

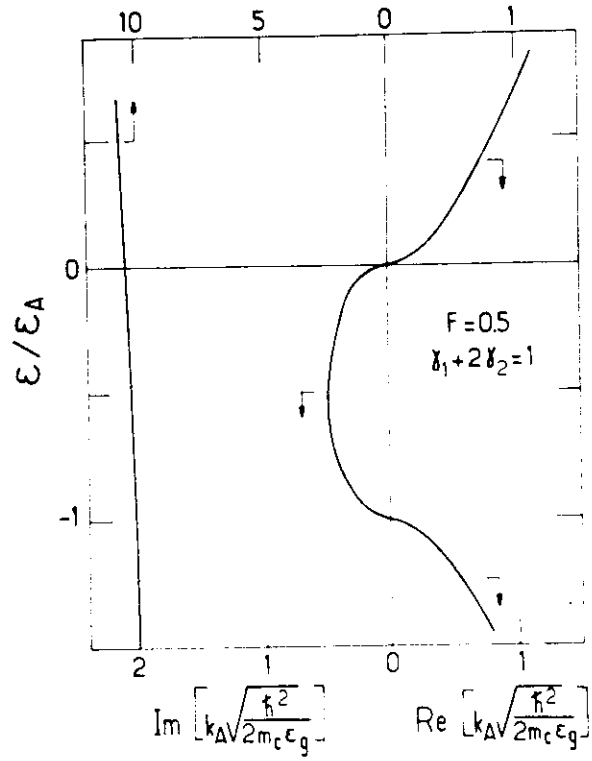

Fig. 11. — Dispersion relations of the light particles states *versus* the real and imaginary wavevectors of a bulk material treated in the Kane model with the remote band effects included up to the second order in $k_\Delta \Delta = \infty$: $F = 0.5$; $\gamma_1 + 2\gamma_2 = 1$; $m_l = 0.067\, m_e$. Notice the different scales for the upper and lower horizontal axis of the left panel.

very large magnitude, eventually larger than the Δ Brillouin zone size along the z axis and ii) is unstable with respect to any change in the small parameters F, $\gamma_1 + 2\gamma_2$. This unphysical solution is a remnent of the remote band and should in fact correspond to their dispersions if they were correctly described (by using a basis much larger than Γ_6 and Γ_8). Clearly, there is no hope of describing the remote bands dispersion relations in the vicinity of Γ_6 and Γ_8, i.e. far from their own edges, by a quadratic law. The wing band seen in figure 11 is just the mathematical transcription of this gross physical inaccuracy. Note however that, in principle, the wing bands are harmless when they correspond to evanescent states which decay very rapidly in space (a few Angströms) on each side of the interfaces. This happens when $F(\gamma_1 - 2\gamma_2) > 0$. They prove troublesome however in the numerical computations. Therefore as the introduction of higher bands adds little physical information to the Γ_1, Γ_7, Γ_8 bands (except of course for the heavy hole band) and produces artefacts like the wing bands, we feel that it is reasonable to get rid of them wherever possible.

II.5 SIMPLIFIED CALCULATIONS OF SUPERLATTICE AND QUANTUM WELL STATES ($\mathbf{k}_{\parallel} = \mathbf{0}$). — At $\mathbf{k}_{\parallel} = \mathbf{0}$, setting F, γ_1, γ_2 equal to zero and discarding the heavy hole line, we obtain a 3×3 first order differential system which can be transformed into a scalar, non-linear in ε, second order differential equation. The latter is obtained by eliminating χ_3 and χ_2 to the benefit of χ_1 in equation (64) (and similarly in the $\underline{D}$ matrix). Proceeding as in Appendix B of the previous chapter, we readily obtain :

$$\left\{ \frac{P^2}{3} p_z \left[\frac{2}{\varepsilon + \varepsilon_A - V_p(z)} + \frac{1}{\varepsilon + \varepsilon_A + \Delta_A - V_\delta(z)} \right] p_z + V_1(z) \right\} \chi_1(z) = \varepsilon \chi_1(z) \tag{68}$$

together with a similar expression for $\chi_3(z)$. The boundary conditions that χ_1 fulfils at the A-B interfaces are such that

$$\chi_1(z) \text{ and } \frac{1}{\mu(\varepsilon, z)} \frac{\mathrm{d}\chi_1}{\mathrm{d}z} \text{ are both continuous} \tag{69}$$

where :

$$\frac{1}{\mu(\varepsilon, z)} = \frac{2P^2}{3} \left[\frac{2}{\varepsilon + \varepsilon_A - V_p(z)} + \frac{1}{\varepsilon + \varepsilon_A + \Delta_A - V_\delta(z)} \right] \tag{70}$$

$\mu(\varepsilon, z)$ is nothing other than the energy-dependent effective mass which appears in the Kane three-band model when the dispersion relations in each kind of layer are written in the implicit form

$$\begin{aligned} \varepsilon &= \frac{\hbar^2 k_A^2}{2\mu_A(\varepsilon)} && \text{in the A layer} \\ \varepsilon &= V_1 - \frac{\hbar^2 k_B^2}{2\mu_B(\varepsilon)} && \text{in the B layer} \end{aligned} \tag{71}$$

the energy being set at the Γ_7 edge of the A material.

We are now in position to calculate the dispersion relations of an A-B superlattice. Let us consider a superlattice unit cell (thickness $d = L_A + L_B$) containing two interfaces. At each interface we apply the continuity conditions given by equation (69). In addition, the band edges $V_1(z)$, $V_p(z)$, $V_\delta(z)$ and the effective mass are periodic functions of z with periodicity d. Thus $\chi_1(z)$ may be written as a Bloch wave :

$$\chi_1(z + d) = \exp(iqd)\, \chi_1(z) \tag{72}$$

with

$$-\frac{\pi}{d} < q \leq \frac{\pi}{d} \tag{73}$$

Inside the A and B layers χ_1 is a linear combination of incoming and outcoming plane waves

$$\chi_1(z) = \alpha \exp(ik_A z) + \beta \exp(-ik_A z); \qquad z \in A$$
$$\chi_1(z) = \gamma \exp(ik_B z) + \delta \exp(-ik_B z); \qquad z \in B \tag{74}$$

Four linear equations are obtained (two boundary conditions per interface) for four unknowns (α, β, γ, δ). These equations can be satisfied only if the determinant of the associated matrix vanishes, which in turn leads to the superlattice dispersion relations.

$$\cos(qd) = \cos(k_A L_A)\cos(k_B L_B) - \frac{1}{2}\left(\xi + \frac{1}{\xi}\right)\sin(k_A L_A)\sin(k_B L_B) \tag{75}$$

with :
$$\xi = \frac{k_A}{\mu_A(\varepsilon)}\frac{\mu_B(\varepsilon)}{k_B} \tag{76}$$

$$\varepsilon(\varepsilon - \varepsilon_A)(\varepsilon - \varepsilon_A + \Delta_A) = \hbar^2 k_A^2 P^2\left(\varepsilon + \varepsilon_A + \frac{2\Delta_A}{3}\right) \tag{77}$$

$$(\varepsilon - V_s)(\varepsilon - V_s + \varepsilon_B)(\varepsilon - V_s + \varepsilon_B + \Delta_B) = \hbar^2 k_B^2 P^2\left(\varepsilon - V_s + \varepsilon_B + \frac{2\Delta_B}{3}\right) \tag{78}$$

Compared with the results obtained in chapter I, we see that the same kind of superlattice dispersion relations are obtained in idealized situations (a single band, a single effective mass etc...) and in the envelope function description of semiconductor superlattices. This is, after all, not very surprising. All our efforts have been put into neglecting the atomic-like details specific to solids. Some of the important features associated with them have, however, survived :

i) the wavevectors k_A and k_B in equations (75-78) are related to the energy *via* expressions which are more complicated than those found in vacuum. This accounts for the multiband nature of solids.

ii) ξ is no longer given by k_A/k_B but should be corrected by the effective mass ratio μ_B/μ_A to account for the effective mass mismatch at the interface.

II.6 MISCELLANEOUS LIMITING CASES.

II.6.1 *Evanescent propagation in one kind of layer. Quantum well bound states.* — Suppose that $V_s > 0$, $V_p < 0$, $V_\delta < 0$ as found in type I heterostructures. Thus for energies ε such that $0 \leq \varepsilon \leq V_s$, $V_p - \varepsilon_A \leq \varepsilon \leq -\varepsilon_A$ or that $V_\delta - \varepsilon_A - \Delta_A \leq \varepsilon \leq -\varepsilon_A - \Delta_A$, the wavevector k_B is imaginary. The corresponding superlattice states are derived from the isolated quantum well levels which, due to the non-zero tunnel coupling across the B layer, have hybridized to form superlattice bands. To obtain their dispersion relations we set $k_B = i\kappa_B$ in equations (75, 76). The quantity ξ

changes into $-i\tilde{\xi}$ and the superlattice dispersion relations becomes :

$$\cos(qd) = \cos(k_A L_A)\cosh(\kappa_B L_B) - \frac{1}{2}\left(\tilde{\xi} - \frac{1}{\tilde{\xi}}\right)\sin(k_A L_A)\sinh(\kappa_B L_B) \quad (79)$$

Morever, if the barrier thickness L_B becomes infinitely thick, suppressing the tunnel coupling between the wells, the isolated quantum well bound states are recovered

$$\cos(k_A L_A) - \frac{1}{2}\left(\tilde{\xi} - \frac{1}{\tilde{\xi}}\right)\sin(k_A L_A) = 0 \quad (80)$$

In equation (80) we have not made use of the parity property of $V_s(z) = V_p(z)$, $V_s(z)$ with respect to the centre of the A layer. If we do so, we easily find that equation (80) factorizes into two equations corresponding to even and odd χ_1's respectively :

$$\cos\left(\frac{1}{2}k_A L_A\right) - \tilde{\xi}\sin\left(\frac{1}{2}k_A L_A\right) = 0$$

$$\cos\left(\frac{1}{2}k_A L_A\right) - \frac{1}{\tilde{\xi}}\sin\left(\frac{1}{2}k_A L_A\right) = 0 \quad (81)$$

It should be noted that these equations are the same as those obtained in the case of the Ben Daniel-Duke quantum well equations (35, 36), except that the masses μ_B, μ_A which enter into equations (80, 81) are energy-dependent. Thus, the quantum well states in host displaying Kane-like bands admit the Ben Daniel-Duke solutions as a limiting case.

II.6.2 *Tight-binding expansion of the superlattice states.* — Let us denote the right hand side of equation (79) by $f(\varepsilon)$. If the barriers are thick, $f(\varepsilon)$ will display large variations and the band widths, which are the energy segments where $|f(\varepsilon)| < 1$ will be narrow. If L_B is infinite we know that the superlattice states reduce to the bound states ε_n of the isolated wells. Thus, in the limit of the thick barriers we may expand $f(\varepsilon)$ in the vicinity of one of these bound states ε_j in order to obtain the superlattice band which originates from the hybridized ε_j's. We find that equation (79) simplifies into :

$$\varepsilon = \varepsilon_j + s_j + 2t_j \cos(qd) \quad (82)$$

with :

$$s_j = -\frac{f(\varepsilon_j)}{f'(\varepsilon_j)} \; ; \qquad 2t_j = \frac{1}{f'(\varepsilon_j)} \quad (83)$$

These are results which are analogous to a tight-binding formulation of a superlattice state. In fact, the shift and transfer integrals s_j and t_j can be analytically obtained in terms of isolated well wavefunctions only. With a tight-binding expansion in mind, let us write the superlattice state as :

$$\chi_1(z) = \frac{1}{\sqrt{2N+1}} \sum_{n=-N}^{+N} \chi_{1,j}(z - nd)\exp(i\,qnd) \; ; \qquad N \to \infty \quad (84)$$

where $\chi_{1j}(z-nd)$ is the j^{th} bound state wavefunction of the well centred at nd. By inserting equation (84) into equation (68), we obtain, after some manipulations,

$$s_j \simeq -2V_s \int_{d-\frac{1}{2}L_A}^{d+\frac{1}{2}L_A} \chi_{1,j}^2(z)\,dz \tag{85}$$

$$t_j \simeq -V_s \int_{-\frac{1}{2}L_A}^{\frac{1}{2}L_A} \chi_{1,j}(z)\,\chi_{1,j}(z-d)\,dz \tag{86}$$

In equations (85, 86) only nearest neighbour interactions have been retained and the non-parabolicity effects have been taken into account only in the evaluation of ε_j. Equations (85, 86) hold for Γ_6-related superlattice states. For light hole states similar expression could be derived with $\chi_{1,j}$ replaced by $\chi_{5,j}$ and V_s by V_p. The orders of magnitude of s_j and t_j are :

$$s_j \simeq -V_s P_b(\varepsilon_j) \exp(-2\kappa_B L_B)[1-\exp(-2\kappa_B L_A)] \tag{87}$$

$$t_j \simeq (-1)^j V_s P_b(\varepsilon_j) \exp(-\kappa_B L_B) \frac{\kappa_B^2}{\kappa_B^2 + k_A^2} \times \left\{1 + \frac{\mu_A(\varepsilon_j)}{\mu_B(\varepsilon_j)} + (-1)^j \left[1 - \frac{\mu_A(\varepsilon_j)}{\mu_B(\varepsilon_j)}\right] \exp(-\kappa_B L_A)\right\} \tag{88}$$

where $j = 1, 2\ldots$; κ_B is the magnitude of the imaginary wavevector in the barrier for the j^{th} bound state of the isolated well and $P_b(\varepsilon_j)$ is the integrated probability of finding the electron in the barrier while in this j^{th} bound state.

Although approximate, equations (87, 88) are helpful for anticipating the trend in superlattice bandwidths and shift integrals with varying barrier or well thicknesses. We notice that s_j decays more rapidly with L_B than t_j. In addition t_j increases in magnitude when ε_j increases, i.e. when the well thickness is decreased for a given j or when dealing with quantum well excited states for a given L_A. Both of these increases are due to decreasing κ_B and increasing P_b. More importantly, we see that t_j and thus the j^{th} bandwidth decrease exponentially with increasing L_B, the decay being controlled by κ_B, i.e. it is faster when V_s, L_A are larger. To a very good accuracy, one may write for the ground superlattice bandwidth ΔE_1

$$\Delta E_1 = V_{eff} \exp(-\kappa_B L_B) \tag{89}$$

Some numerical examples will be given below (section II.7)

II.6.3 *Propagating states in both kinds of layers.* — We have seen that the superlattice states corresponding to the imaginary wavevectors in one kind of layer can be analyzed in terms of hybridized bound levels of isolated wells. It could be asked if a similar link can be established between the superlattice states which propagate in both kinds of layers (i.e. k_A, k_B real, which means $\varepsilon \geq V_s$,

$\varepsilon \leqslant -\varepsilon_A - V_p$, $\varepsilon \leqslant -\varepsilon_A - \Delta_A - V_\delta$ in type I heterostructures) and certain continuum states of isolated wells. We recall that the continuum of a single quantum well is not structureless (see chapter I). On the contrary, virtual bound states take place in the continuum when

$$k_A L_A = p\,\pi\ ; \qquad p = 1, 2... \tag{90}$$

The virtual bound states are the continuation of the true quantum well bound states when their confinement energies exceed the barrier height. Both true and virtual bound states are matched at the onset of the continuum : it can immediately be checked that equation (90), with k_A given by equation (77) in terms of the energies corresponding to the onset of a continuum (i.e. $\varepsilon = V_s$, $\varepsilon = -\varepsilon_A + V_p$, $\varepsilon = -\varepsilon_A - \Delta_A + V_\delta$) is indeed a solution of the quantum well bound state equation (at the onset of the continuum $\kappa_B \to 0$ and $\tilde{\xi}$ diverges in Eq. (80)).

By examining equation (75) we notice that the energy of a virtual bound level of an isolated well always corresponds to an allowed superlattice state with q equal to

$$q = \pm \left(k_B \frac{L_B}{L_A + L_B} + \frac{p\,\pi}{L_A + L_B} \right) \tag{91}$$

To some extent therefore, the superlattice states which propagate in each kind of layer can be viewed as the hybridization of the virtual bound levels of the isolated wells.

II.6.4 *Heavy hole superlattice states.* — If we were to use our simplified Kane model, the heavy hole superlattice states would be dispersionless and only the energies $-\varepsilon_A$, $-\varepsilon_A + V_p$ would be allowed. However since the heavy holes decouple from the light particles states, we can re-introduce the coupling between Γ_{8h} and the remote bands to correctly describe the heavy hole curvature. The problem becomes identical to a Ben Daniel-Duke one because the heavy hole envelope functions are the eigenfunctions of :

$$\left[-\varepsilon_A - p_z \frac{1}{2M_{hh}(z)} p_z + V_p(z) \right] \chi_3(z) = \varepsilon \chi_3(z) \tag{92}$$

$$V_p(z + d) = V_p(z) \tag{93}$$

where : $$\frac{m_0}{M_{hh}^{(A)}} = \gamma_1^{(A)} - 2\gamma_2^{(A)}\ ; \quad \frac{m_0}{M_{hh}^{(B)}} = \gamma_1^{(B)} - 2\gamma_2^{(B)} \tag{94}$$

We can proceed along the same lines as before to calculate $\chi_3(z)$. Writing $\chi_3(z)$ as the sum of the incoming and outgoing plane waves in each kind of layer, we obtain the heavy hole superlattice states in the same form as equation (75), except that :

$$\xi = \frac{k_A}{M_{hh}^{(A)}} \frac{M_{hh}^{(B)}}{k_B} \tag{95}$$

for heavy holes. In equation (95), there is

$$k_A = \sqrt{\frac{2M_{hh}^{(A)}}{\hbar^2}[-\varepsilon_A - \varepsilon]}; \qquad k_B = \sqrt{\frac{2M_{hh}^{(B)}}{\hbar^2}[-\varepsilon_A - \varepsilon + V_p]} \tag{96}$$

In the energy segment $-\varepsilon_A + V_p < \varepsilon < -\varepsilon_A$, one of the wavevectors (Eq (96)) becomes imaginary (say k_B). In this case equation (75) should be replaced by equation (79), k_B by $i\kappa_B$ and ξ by $-\tilde{\xi}$. Qualitatively therefore both light particle and heavy hole superlattice states are quite similar. Quantitatively, however, the heavy hole superlattice bands are much narrower than the light particle ones due to the larger heavy hole mass. For numerical examples, see section (II.7).

II.7 SPECIFIC EXAMPLES. — To substantiate the previous considerations figures (12-20) present the calculated energy levels of several quantum wells and superlatttices.

Quantum wells

The dominant effect in quantum well energy levels is the finiteness of the barrier height. This is illustrated in figures (12-15) in the case of GaAs-Ga(Al)As where we have plotted :

i) the dependence of the confinement energies E_1, LH_1, HH_1 of the ground bound states upon the barrier height V_s and $|V_p|$ for electron, light and heavy holes

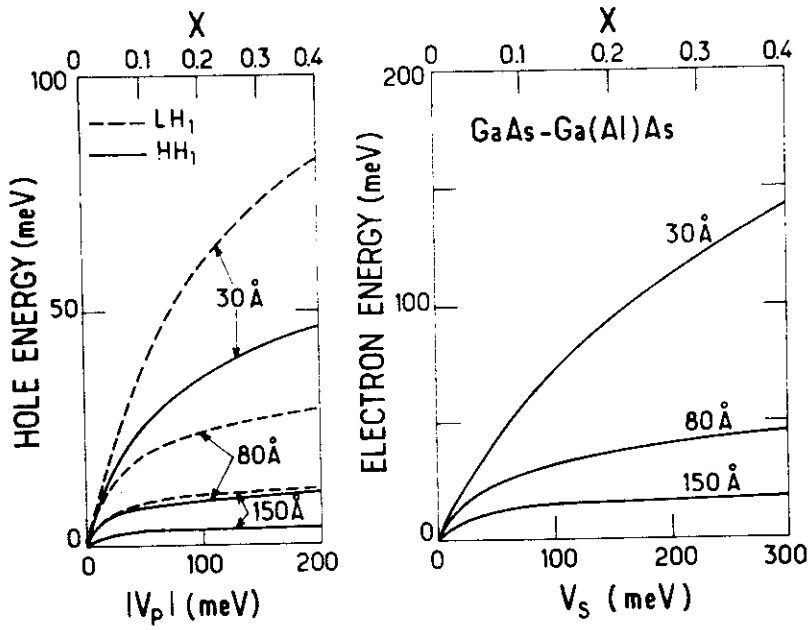

Fig. 12. — Evolution of the ground states for electron (E_1), heavy hole (HH_1) and light hole (LH_1) *versus* the barrier heights V_s and $|V_p|$ in GaAs-Ga(Al)As quantum wells. Three well thicknesses have been considered L = 30 Å, 80 Å and 150 Å respectively.

respectively, i.e. upon the Al mole fraction x, for three GaAs slab thicknesses : L = 30 Å, 80 Å and 150 Å respectively. The calculations have been performed using a 60 % – 40 % split between the conduction and valence bands of the bandgap energy difference ΔE_g between $Ga_{1-x}Al_xAs$ and GaAs. Taking

$$\Delta E_g(x) = 1247\, x \text{ meV} \tag{97}$$

we are left with

$$V_c(x) = 748.2\, x \text{ meV} \tag{98}$$

$$V_p(x) = -498.8\, x \text{ meV} \tag{99}$$

Figure 12 shows that the asymptotic values of E_1, LH_1, HH_1, which correspond to a perfect confinement (i.e. $k_A L = \pi$, where k_A is the appropriate wavevector in GaAs), are barely obtained, apart from heavy holes in thick ($L > 100$ Å) wells. On

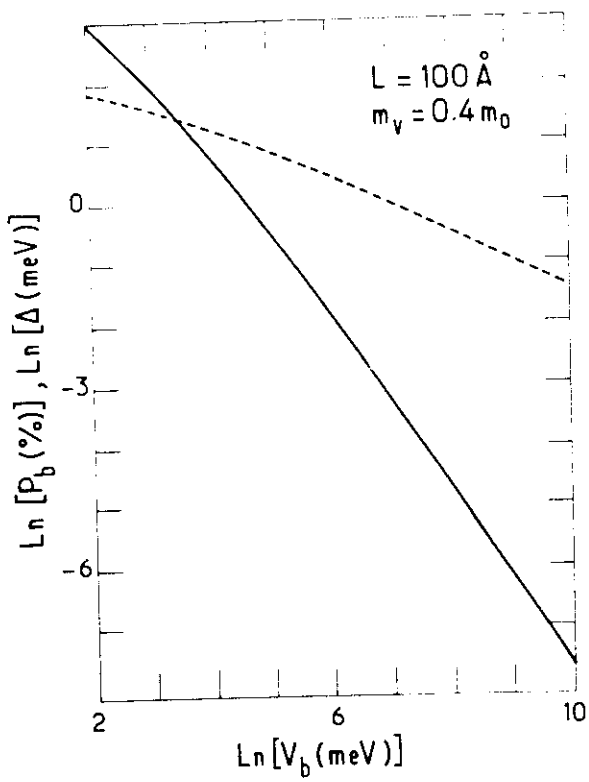

Fig. 13. — The natural logarithms of the energy difference $\Delta = \dfrac{\hbar^2\pi^2}{2M_{hh}L^2} - HH_1$ (dashed line) and of the integrated probability P_b of finding the hole in the barriers (solid line) are plotted *versus* the hole barrier height $(-V_p)$ for a quantum well thickness L = 100 Å. $M_{hh} = 0.4\, m_0$.

the one hand, it should be noticed that a better justification can be obtained for the same approximation (i.e. perfect confinement) in the case of the wavefunction. This is illustrated in figure 13 for heavy holes and can be analytically traced back. The convergence of $E_1(HH_1, LH_1)$ towards $\hbar^2\pi^2/2m\,L^2$, where m is the effective mass appropriate for the electrons (light hole, heavy hole), is slow since it is proportional to $V_s^{-1/2}(|V_p|^{-1/2})$. On the other hand, the spatial confinement of the carrier in the well is completed more rapidly : the integrated probability of finding the particle outside the well drops to zero like $V_s^{-3/2}(|V_p|^{-3/2})$.

ii) the energy level diagrams *versus* the GaAs slab thickness L for an Al mole fraction of 0.3 (Figs. 14, 15). The solid lines represent the true quantum well bound states whereas the dashed lines represent the locii of the virtual bound states (or transmission resonances) which fulfil

$$k_A(\varepsilon_p)\,L = p\pi\,; \qquad p = 1, 2, \ldots \tag{100}$$

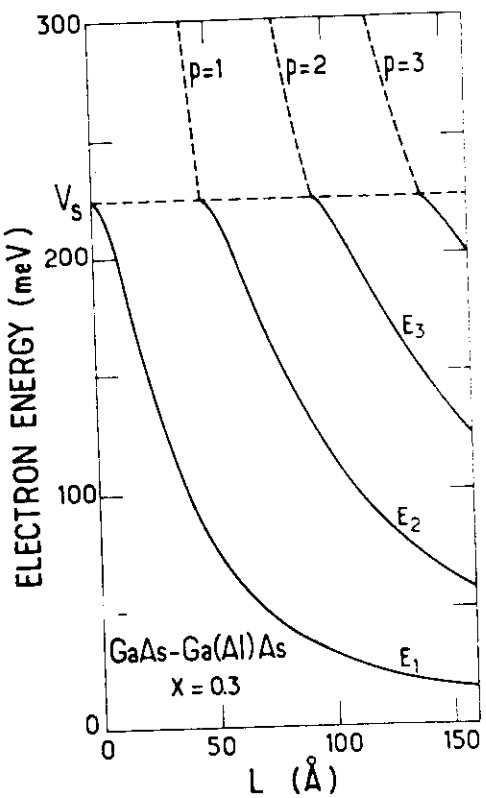

Fig. 14. — Energy level diagram for electrons in GaAs-$Ga_{0.7}Al_{0.3}As$ quantum wells *versus* the GaAs slab thickness. The solid lines correspond to bound states and the dashed lines to virtual bound states. V_s = 224.5 meV.

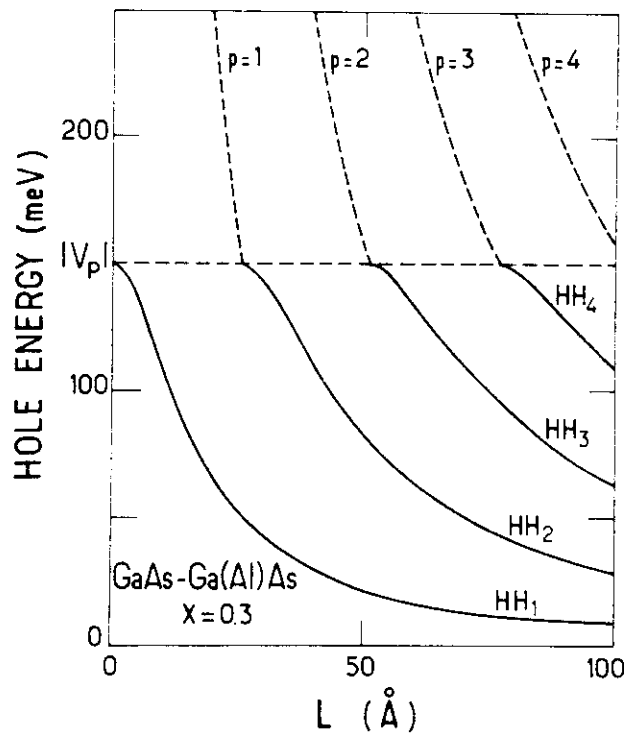

Fig. 15. — Energy level diagram for heavy holes in $Ga_{1-x}Al_xAs$ quantum wells *versus* the GaAs slab thickness. The solid lines correspond to bound states and the dashed lines to virtual bound states. $|V_p| = 149.6$ meV. $M_{hh}^{GaAs} = 0.38\, m_0$. $M_{hh}^{Ga_{0.7}Al_{0.3}As} = 0.45\, m_0$.

for energies exceeding the top of the confining barrier. In equation (100) k_1 denotes the carrier wavevector inside the well. It is related to ε_p either by equation (77) (light particle) or by equation (96) (heavy hole). It should be pointed out that semiconductor quantum wells always admit one bound state, as the ground states $E_1(HH_1, LH_1)$ only reach the top of their respective barriers at $L = 0$.

The band non-parabolicity, which only affects the light particle states, plays a relatively minor part in GaAs-Ga(Al)As quantum wells. This is due to the large GaAs bandgap. Basically speaking, band non-parabolicity amounts to replacing the GaAs band edge mass by an energy-dependent mass whose relative increment is equal to the ratio between the kinetic energy and the bandgap. As the confinement energy varies roughly in the same way as the inverse of the carrier effective mass, one expects a non-parabolicity-induced correction of the order of the confinement energy (calculated with the band edge mass) divided by the GaAs bandgap. This qualitative prediction is more or less supported by the calculations.

Obviously, the smaller the well-acting material bandgaps, the larger the non-parabolicity effects. Again, qualitatively, the non-parabolicity effects scale the same

way as ε_A^{-2} because the band edge mass itself is proportional to ε_A. Therefore, the non-parabolicity is more important in the evaluation of the electron confinement energies of $Ga_{0.47}In_{0.53}$ As-InP or GaSb-AlSb quantum wells than in GaAs-Ga(Al)As ones. Also it is more important for excited levels than for the ground states.

Superlattices

The superlattice states corresponding to evanescent propagation in one kind of layer present few surprises (Figs. 16-18). One notices that the isolated quantum well levels broaden to form the superlattice bands. Their widths increase i) when the well-acting layer narrows at a fixed barrier thickness, ii) when at fixed L_A, L_B one looks at the bands originating from the excited levels of the isolated quantum wells, and iii) when, at fixed L_A, the barrier thickness decreases.

As anticipated in our tight-binding description of the superlattice states, the E_1 bandwidth decays exponentially with the barrier thickness (Fig. 19). Furthermore, it is clear from figures 16 and 18 that the superlattice bandwidth decreases with the increasing carrier effective mass, to the point where the heavy hole bandwidths are almost negligible for $L_A \geq 100$ Å.

The pattern of the superlattice bands which originate from the propagating states in both kinds of layers is perhaps more intricate. This is particularly clear for the

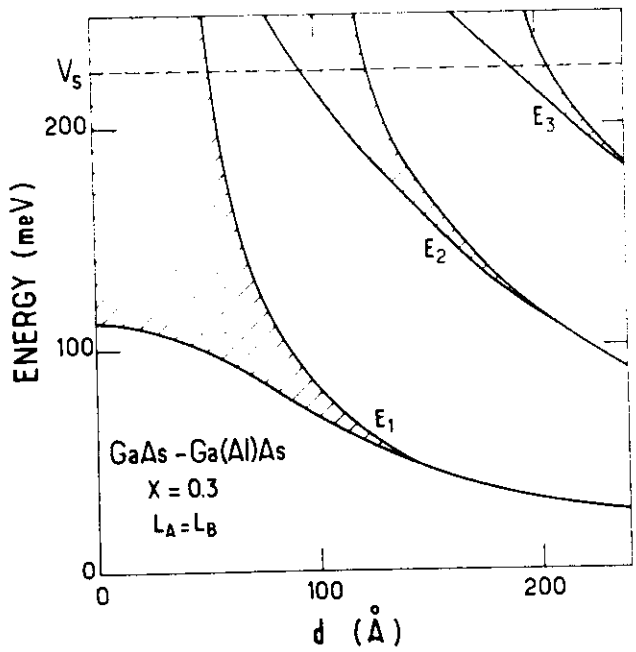

Fig. 16. — Superlattice band structure for electrons in GaAs-$Ga_{0.7}Al_{0.3}As$ superlattices *versus* period d. Equal layer thicknesses are assumed in the calculations. The allowed energy states are hatched.

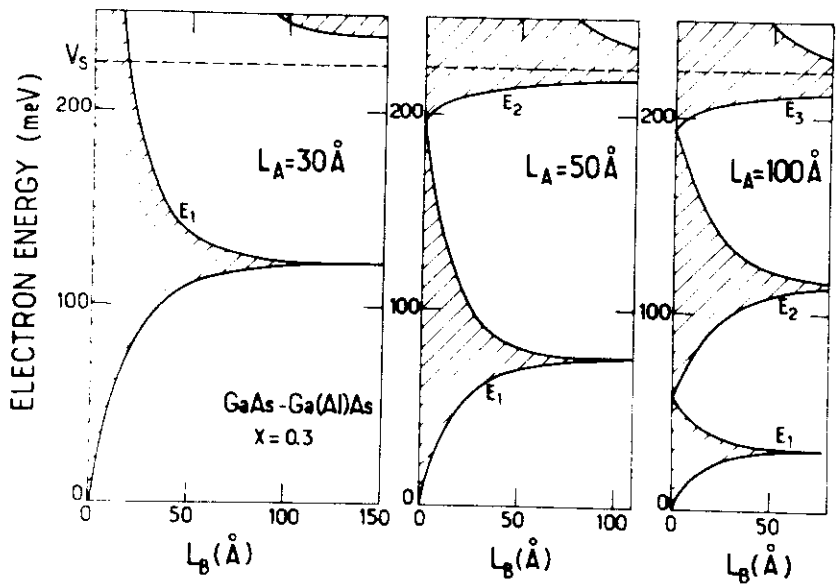

Fig. 17. — Evolution of the superlattice band structure for electrons in GaAs-$Ga_{0.7}$-$Al_{0.3}$As superlattices when the $Ga_{0.7}$-$Al_{0.3}$As layer thickness L_B is increased and the GaAs layer thickness L_A is kept fixed. The allowed energy states are hatched.

heavy hole bands (Fig. 18) where a fairly complex band pattern above the barrier height constrasts with the simple features found below $|V_p|$. In particular, the bands HH_2 and HH_3 cross at one point, as do HH_3 and HH_4 etc... It is possible to check that these degeneracy points take place when both $k_A L_A$ and $k_B L_B$ are integer multiples of π. For these particular energies and thicknesses there is a Fabry-Pérot effect for the hole waves in *both* kinds of layers. It can be inferred from this particular example that the superlattice states which correspond to the propagating states in both kinds of layers should strongly depend upon the barrier thickness L_B, while those originating from the hybridization of quantum well bound states are less dependent upon this quantity.

The InAs-GaSb superlattices are the extreme case of type II heterostructures [30]. The latter are characterized by the fact that V_s and V_p have the same sign, so that one kind of layer attracts electrons whereas the other kind is a potential well for the holes. In InAs-GaSb the top of the GaSb valence band is located in energy above the bottom of the InAs conduction band. When the superlattice period increases, as L_A is equal to L_B, the E_1 band moves towards the InAs conduction band edge while HH_1 approaches the top of the GaSb valence band. There should thus exist a critical period d_c beyond which HH_1 is located at a higher energy than E_1 (Fig. 20). This situation is, to our knowledge, unique in semiconductor superlattices. For $d \geq d_c$ one should expect some kind of a semiconductor $\rightarrow$ semimetal transition whereby electrons flow from the GaSb to the InAs layers leaving holes behind them.

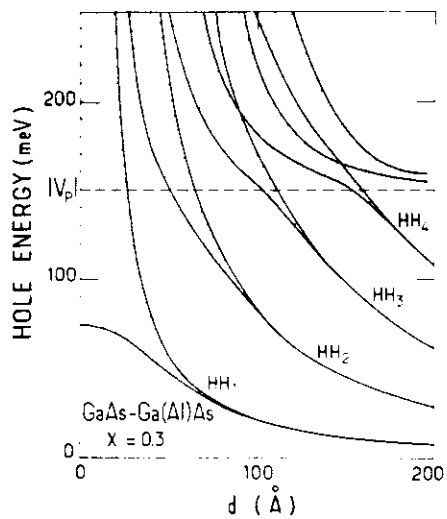

Fig. 18. — Superlattice band structure for heavy holes in GaAs-$Ga_{0.7}Al_{0.3}As$ superlattices *versus* period d. Equal layer thicknesses are assumed in the calculations. The allowed energy states are hatched.

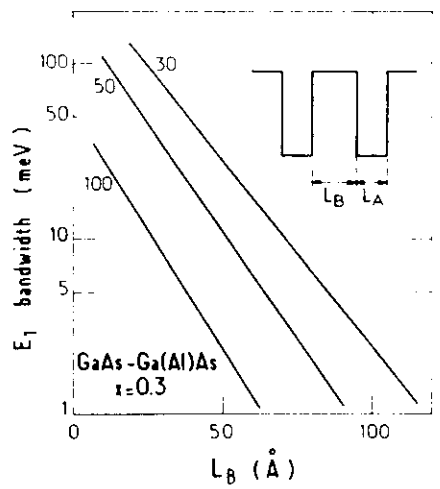

Fig. 19. — The E_1 bandwidth is plotted *versus* the $Ga_{0.7}Al_{0.3}As$ layer thickness L_B in GaAs-$Ga_{0.7}Al_{0.3}As$ superlattices with three different GaAs layer thicknesses (30 Å, 50 Å, 100 Å). Notice the logarithmic scale for the E_1 bandwidth.

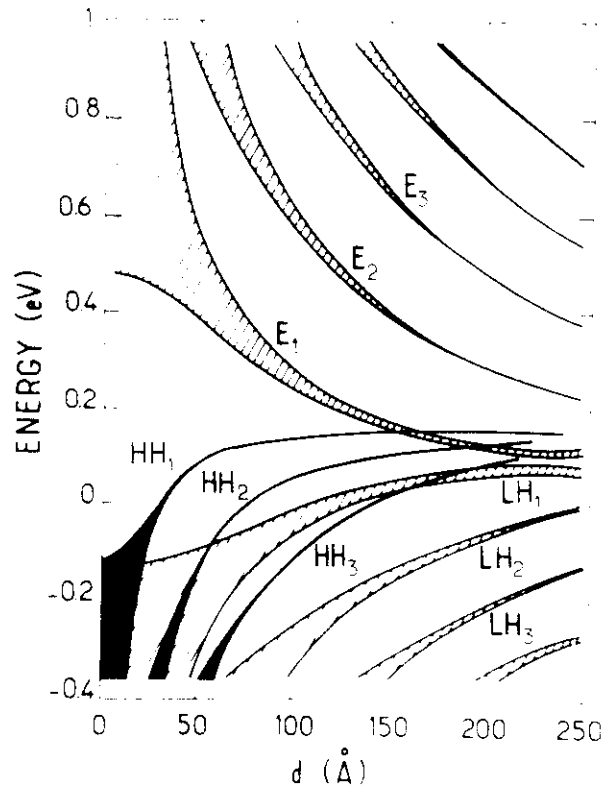

Fig. 20. — Evolution of the InAs-GaSb superlattice band structure with increasing period d ($L_x = L_y$). The allowed energy levels are hatched (light particles) or black (heavy holes). The energy zero is taken at the bottom of the bulk InAs conduction band.

Actually, the situation is more complicated since the band crossings which take place at $\boldsymbol{k}_{\perp} = \mathbf{0}$ are replaced by anticrossings if the in plane wavevector is non zero [2, 32]. This leads to the formation of small gaps between E_1 and HH_1. Our present knowledge of this fascinating system is still incomplete as the combination of technological problems (residual impurities in InAs and GaSb layers) and theoretical complexity (non-negligible stress effects due to the imperfect lattice matching, charge redistribution between InAs and GaSb layers, many-body effects ?) conspire to elude clear cut answers.

II.8. LABELLING AND COUNTING SUPERLATTICE STATES. — A superlattice state is labelled by two wavevectors : $q\hat{\boldsymbol{z}}$ and $\boldsymbol{k}_{\perp}$ (which express the delocalized nature of the wavefunctions along and perpendicular to the growth axis), and by a subband index n ($n = 1, 2...$). A label E, HH LH... is also affixed to a superlattice state to indicate from which host band the superlattice state is principally derived. Notice that this

label has little physical meaning if significant band mixing occurs in the host layer. This happens at $\boldsymbol{k}_{\perp} = \mathbf{0}$ if the host bandgaps are very narrow or in the Γ_6 bands at $\boldsymbol{k}_{\perp} \neq \mathbf{0}$ (see below). In addition, there is a "spin" quantum number which can take two values $\left(\text{say} \pm \frac{1}{2}\right)$ and which reduces to the z component of the spin quantum number σ_z if there are no spin-orbit effects. Due to the finite spin-orbit splitting, σ_z is no longer a good quantum number. However, each state of the Hamiltonian (Eq. (16)) remains twice degenerate at $\boldsymbol{k}_{\perp} = \mathbf{0}$ (since the inversion asymmetry terms have been omitted). This Kramers degeneracy is a direct consequence of the invariance of $\underset{\sim}{D}^{(0)} + \varphi(\boldsymbol{r})\,\underset{\sim}{1}$ under a time-reversal operation [23]. We shall see in section III that this twofold degeneracy is lifted in heterostructures which lack inversion symmetry. This happens for instance when $\varphi(z) \neq \varphi(-z)$ (asymmetric band bending) or $V_c(z) \neq V_c(-z)$ etc... (asymmetrically designed heterostructures).

We have seen that the superlattice states are Bloch waves (Eq. (72)). Assuming that the superlattice is made of an infinite sequence of blocks containing N superlattice periods where N is very large, we may apply the Born-von Karman boundary conditions, i.e. we require the superlattice wavefunction to be the same at both ends of a given block :

$$\chi_q(z + Nd) = \chi_q(z) \tag{101}$$

or : $$qNd = 2\pi p \qquad p = 0, 1, 2, \ldots N - 1 \tag{102}$$

Thus, there are N independent q values, i.e. as many q values as superlattice unit cells in a block. These q values are equidistant and separated from each other by $\frac{2\pi}{Nd}$. Any summations of the form $\sum_q \alpha(q)$ will be converted into an integration :

$$\sum_q \alpha(q) \to \frac{Nd}{2\pi} \int_{\text{BZ}} \alpha(q)\, \mathrm{d}q \tag{103}$$

The upper and lower limits of the integral can be any number provided they differ by $\frac{2\pi}{d}$, i.e. the size of the superlattice Brillouin zone along the growth axis. Often the segment $\left[-\frac{\pi}{d} + \frac{\pi}{d}\right]$ is chosen to emphasize the parity property

$$\varepsilon(q) = \varepsilon(-q) \tag{104}$$

fulfilled by any superlattice band.

III. In-plane dispersions in semiconductor heterostructures.

When the in-plane wavevector $\boldsymbol{k}_{\perp}$ is not equal to zero, the heavy hole and light particle states become coupled. This is simply the consequence of the degenerate nature of the Γ_8 hosts' band edges, which originates from the P symmetry of the orbital parts of the band edge Bloch functions. In fact, even the simplest (i.e.

isotropic) quadratic Hamiltonian for Γ_8 bands in a bulk material is not a scalar, which is the case for Γ_6 bands (S symmetry). As shown by Luttinger [22] the isotropic Γ_8 Hamiltonian should be written :

$$\mathcal{H} = \alpha k^2 - \beta(\boldsymbol{k}.\boldsymbol{J})^2 \tag{105}$$

where $\boldsymbol{J}$ is the total angular momentum $\left(J = \frac{3}{2}\right)$. From equation (105) it can be seen that, if the $\boldsymbol{J}$ quantization axis is given (say the $\hat{\boldsymbol{z}}$ axis), the decoupling between the $m_J = \pm\frac{3}{2}$ and $m_J = \pm\frac{1}{2}$ states is only possible if $\boldsymbol{k} /\!/ \boldsymbol{J} /\!/ \hat{\boldsymbol{z}}$ while, if $\boldsymbol{k}$ is arbitrary, the eigenstates of equation (105) are no longer eigenfunctions of J_z. However, it is always possible to rotate the reference frame in a bulk material in such a way that the new direction z along which $\boldsymbol{J}$ will be quantized coincides with $\boldsymbol{k}$, thus obtaining the simultaneous diagonalizations of J_z and $\mathcal{H}$.

In heterostructures the potential term $V(z)\,\mathbb{1}$, which should be added to the right hand side of equation (105), gives rise to anisotropy. The interface planes have the simple expressions z = constant and the wavefunctions are separable in z and (x, y). If we quantize $\boldsymbol{J}$ along the growth axis, which is what we did in section II, the $m_J = \pm\frac{3}{2}$ and $m_J = \pm\frac{1}{2}$ states become decoupled if $\boldsymbol{k} /\!/ \boldsymbol{J}$, i.e. if $\boldsymbol{k}_- = \boldsymbol{0}$. If $\boldsymbol{k}_- \neq \boldsymbol{0}$ light particle and heavy hole states will hybridize. However, contrary to the bulk case, $\boldsymbol{J}$ can no longer be rotated to line up along $\boldsymbol{k}$, thereby recovering a simple situation. This is because $\boldsymbol{k}$ is no longer a good quantum number due to the potential term $V(z)\,\mathbb{1}$. If we attempt to rotate the (xyz) frame to obtain a (XYZ) frame where Z and J_Z are parallel to $\boldsymbol{k}_A$ (the carrier wavevector in the A material), it will not lead to the lining up between $\boldsymbol{J}$ and $\boldsymbol{k}_B$ (the carrier wavevector in the B material). The decoupling will thus never be complete. The best one can do is to choose a $\boldsymbol{J}$ quantization axis which renders the valence Hamiltonian less complicated. To quantize $\boldsymbol{J}$ along the growth axis seems the most natural choice. However, if band warping is neglected, significant simplifications are obtained by quantizing $\boldsymbol{J}$ in a direction perpendicular to the growth axis [2]. Obviously, if we add the Γ_8 band warping (i.e. the non-sphericity) to equation (105) and include the Γ_6 edge in the analysis (to account for non-parabolicity) the complexity is increased, making it impossible to obtain analytical results. To our knowledge, the only circumstances where analytical results for which Γ_6 or Γ_8 in-plane dispersions have been obtained are :

i) Γ_8 eigenstates of a quadratic Hamiltonian (like Eq. (105)) and infinite barrier heights [31].

ii) Γ_6 in-plane dispersions for a Ben Daniel-Duke problem (see section II.3).

iii) in-plane dispersions of the light particle states of a Kane Hamiltonian with the remote band effects neglected [4] but otherwise V_s, V_p steps of arbitrary height.

The numerical solutions of the 6×6 heterostructure Hamiltonian (i.e. including Γ_6 and Γ_8 bands and the remote band treated up to the second order in $\boldsymbol{k}$) have been extensively discussed by Altarelli *et al.* [2, 33, 34]. Under flat band

conditions an exact solution to the problem can be found [32] along the lines previously discussed. One simply expresses the fact that, in each kind of layer, the heterostructure state is a linear combination of propagating (or evanescent) bulk states. The energy ε and the in-plane wavevector $\boldsymbol{k}_\perp$ having been given, $k_z^{(A)}$ and $k_z^{(B)}$ can then be univoquely determined, together with the envelope function χ which is a 6×1 column vector. The unknown coefficients of the linear combination are then obtained by writing the continuity of χ and $\underset{\sim}{A}\chi$ (Eq. (21)) across the A-B interfaces. In figures 21 and 22 we show the results of such calculations performed for a 70 Å - 70 Å and a 100 Å - 100 Å InAs-GaSb superlatttice [32]. The first superlattice has simpler in-plane dispersions : there is no overlap

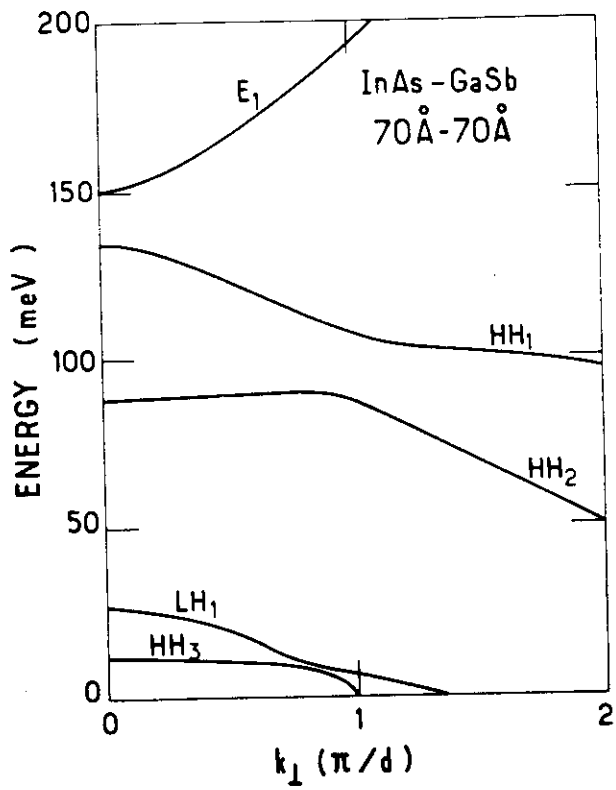

Fig. 21. — In-plane dispersion relations for a 70 Å-70 Å InAs-GaSb superlattice obtained in the 6 band model. $q = 0$. $\varepsilon_A = 0.42$ eV ; $m_{\Gamma_6}^{(A)} = 0.023\, m_0$; $\varepsilon_B = 0.81$ eV ; $\gamma_1^{(A)} = \gamma_1^{(B)} = 3.7$; $\gamma_2^{(A)} = \gamma_2^{(B)} = \gamma_3^{(A)} = \gamma_3^{(B)} = 0.6$. The energy zero has been taken at the bottom of the bulk InAs conduction band. Courtesy of J.M. Berroir [32].

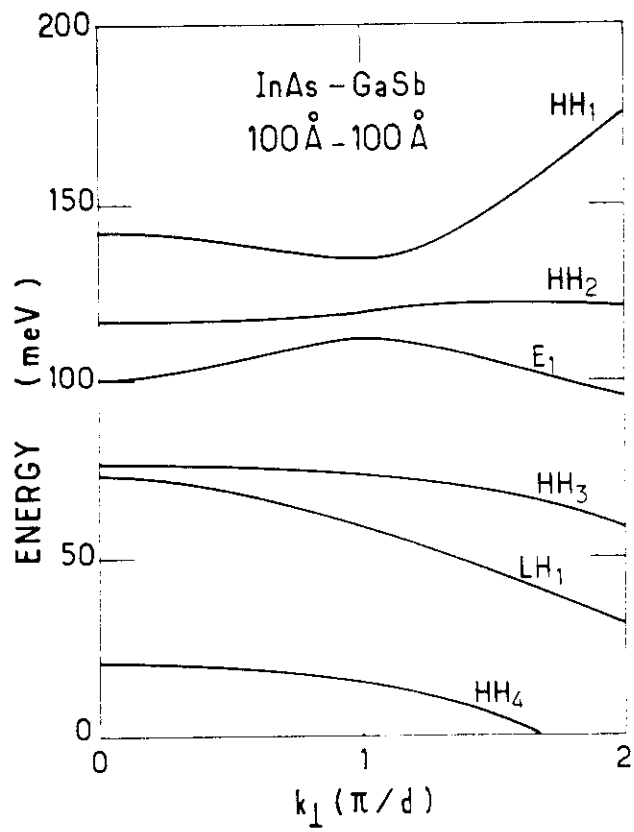

Fig. 22. — In-plane dispersion relations for a 100 A-100 A InAs-GaSb superlattice obtained in the 6 band model. Flat band conditions have been assumed. The band parameters used in the calculations are the same as in figure 21. $q = 0$. Courtesy of J.M. Berroir [32].

between E_1 and HH_1 for any q or any $\mathbf{k}_\perp$. The 100 Å - 100 Å superlattice is such that at $q = 0$, $\mathbf{k}_\perp = \mathbf{0}$, $E_1 < HH_1$, HH_2. However, as soon as $\mathbf{k}_\perp \neq \mathbf{0}$ a strong mixing occurs between E_1 and the heavy hole states. As a result, E_1 and HH_1, HH_2 anti-cross thus preventing the formation of a true semi-metallic phase. Notice that the calculations are not self-consistent in the 100 Å - 100 Å case as the charge redistributions in a superlattice unit cell and their associated band bendings were not taken into account.

The in-plane dispersions of Γ_8 subbands in GaAs-Ga(Al)As heterostructures are the subject of active research [5, 32, 37]. In these materials the coupling with the Γ_6 bands is relatively weak and a parabolic description of the host bands is reasonable. Neglecting once more the inversion-asymmetry splitting, the valence

band Hamiltonian takes the form

$$\mathscr{H}_{\Gamma_8} = \begin{matrix} \left\langle \frac{3}{2}, \frac{3}{2} \right| \\ \left\langle \frac{3}{2}, -\frac{1}{2} \right| \\ \left\langle \frac{3}{2}, \frac{1}{2} \right| \\ \left\langle \frac{3}{2}, -\frac{3}{2} \right| \end{matrix} \begin{bmatrix} \mathscr{H}_{hh} & c & b & 0 \\ c^* & \mathscr{H}_{lh} & 0 & -b \\ b^* & 0 & \mathscr{H}_{lh} & c \\ 0 & -b^* & c^* & \mathscr{H}_{hh} \end{bmatrix} \tag{106}$$

where :

$$\mathscr{H}_{hh} = -\frac{1}{2m_0} p_z(\gamma_1 - 2\gamma_2) p_z + V_p(z) - \frac{\hbar^2 k_\perp^2}{2m_0}(\gamma_1 + \gamma_2) \tag{107}$$

$$\mathscr{H}_{lh} = -\frac{1}{2m_0} p_z(\gamma_1 + 2\gamma_2) p_z + V_p(z) - \frac{\hbar^2 k_\perp^2}{2m_0}(\gamma_1 - \gamma_2) \tag{108}$$

$$c(\boldsymbol{k}_\perp) = \frac{\hbar^2}{m_0}\frac{\sqrt{3}}{2}\left[\gamma_2(k_x^2 - k_y^2) - 2i\gamma_3 k_x k_y\right] \tag{109}$$

$$b(\boldsymbol{k}_\perp, p_z) = \frac{\sqrt{3}}{2}\frac{\hbar}{m_0}(k_x - ik_y)(\gamma_3 p_z + p_z \gamma_3) \tag{110}$$

In equations (107, 110) the γ's are the Luttinger parameters which describe the coupling between Γ_8 and all the hosts' edges, including Γ_6. These parameters are, in principle, position-dependent (since they are different in the A and B layers). Consequently the terms of the form γp_z have been symmetrized.

We notice that, as expected, the b and c terms vanish if $\boldsymbol{k}_\perp \neq \boldsymbol{0}$. If they were always negligible the Γ_8 Hamiltonian would split into two independent Ben Daniel-Duke Hamiltonians : one for the heavy holes $\left(m_J = \pm\frac{3}{2}\right)$ and one for the light holes $\left(m_J = \pm\frac{1}{2}\right)$. This zeroth order approximation, hereafter termed the diagonal approximation, is characterized by a mass reversal effect, i.e. the heavy hole effective mass is heavy along $\hat{\boldsymbol{z}}$ but light in the layer plane whereas the light hole effective mass is light along $\hat{\boldsymbol{z}}$ but heavy in the layer plane. This means that in the diagonal approximation the subbands HH_n and LH_n should cross. Such crossings are suppressed by the non-vanishing b and c terms and replaced by anti-crossings. In the following we shall keep the notations LH_n, HH_n to label the valence subbands, although it should be kept in mind that they retain little physical significance if $\boldsymbol{k}_\perp \neq \boldsymbol{0}$. The b and c terms very effectively mix the $\boldsymbol{k}_\perp \neq \boldsymbol{0}$ solutions.

The eigenstates of equation (106) are twice degenerate if $V_p(z)$ (and $-e\varphi(z)$ if there is a band bending) and the γ's are even functions of z. This can be explicitly shown at small $\boldsymbol{k}_\perp$ by eliminating the $\pm\frac{1}{2}$ components of the eigenstates of equation

(106) to the benefit of the $\pm \frac{3}{2}$ ones and by writing the effective 2×2 Hamiltonian which acts on the $\pm \frac{3}{2}$ components as :

$$\underset{\sim}{\mathscr{H}}_{\text{eff}} \begin{bmatrix} \psi_{3/2} \\ \psi_{-3/2} \end{bmatrix} = \begin{bmatrix} \mathscr{H}_+ & W \\ W^* & \mathscr{H}_- \end{bmatrix} \begin{bmatrix} \psi_{3/2} \\ \psi_{-3/2} \end{bmatrix} = \varepsilon \begin{bmatrix} \psi_{3/2} \\ \psi_{-3/2} \end{bmatrix} \tag{111}$$

where :

$$\mathscr{H}_+ = \mathscr{H}_{hh} + c \frac{1}{\varepsilon - \mathscr{H}_{lh}} c^* + b \frac{1}{\varepsilon - \mathscr{H}_{lh}} b^* \tag{112}$$

$$\mathscr{H}_- = \mathscr{H}_{hh} + c^* \frac{1}{\varepsilon - \mathscr{H}_{lh}} c + b^* \frac{1}{\varepsilon - \mathscr{H}_{lh}} b \tag{113}$$

$$W = b \frac{1}{\varepsilon - \mathscr{H}_{lh}} c - c \frac{1}{\varepsilon - \mathscr{H}_{lh}} b \tag{114}$$

or more explicitly

$$W = \frac{3\hbar^2}{4m_0^2} (k_x - i k_y) \left\{ (\gamma_3 p_z + p_z \gamma_3) \frac{1}{\varepsilon - \mathscr{H}_{lh}} [\gamma_2 (k_x^2 - k_y^2) - 2i \gamma_3 k_x k_y] - \right.$$
$$\left. - [\gamma_2 (k_x^2 - k_y^2) - 2i \gamma_3 k_x k_y] \frac{1}{\varepsilon - \mathscr{H}_{lh}} (\gamma_3 p_z + p_z \gamma_3) \right\} \tag{115}$$

At $\boldsymbol{k}_\perp = \mathbf{0}$ the spectrum of $\mathscr{H}_{\text{eff}}$ is twice degenerate. The eigenstates of equation (111) are :

$$\boldsymbol{\psi}_{-3/2}^{(n)} = \begin{bmatrix} 0 \\ \chi_n(z) \end{bmatrix} ; \qquad \boldsymbol{\psi}_{3/2}^{(n)} = \begin{bmatrix} \chi_n(z) \\ 0 \end{bmatrix} \tag{116}$$

where the χ_n's are the $\boldsymbol{k}_\perp = \mathbf{0}$ -heavy hole eigenfunctions. If $\boldsymbol{k}_\perp$ is small, the $\boldsymbol{k}_\perp$-dependent contributions to $\mathscr{H}_+$ and $\mathscr{H}_-$ and the W term will also be small as they involve at least second and third powers of k_x, k_y respectively. We can therefore attempt a diagonalization of the $\boldsymbol{k}_\perp$-dependent contributions within the 2×2 subspace, spanned by the degenerate $\boldsymbol{\psi}_{-3/2}^{(n)}$ and $\boldsymbol{\psi}_{-3/2}^{(n)}$ eigenstates, and neglect all the admixtures with the other $\boldsymbol{\psi}_{-3/2}^{(m)}$, $\boldsymbol{\psi}_{-3/2}^{(m)}$ states. We readily obtain :

$$\varepsilon = \varepsilon_n \pm | \langle \chi_n | W | \chi_n \rangle | \tag{117}$$

where ε_n is the mean values of $\mathscr{H}_+$ or $\mathscr{H}_-$ over χ_n. Equation (117) is in fact an implicit equation for ε, inasmuch as ε_n and W are energy dependent and involve an infinite number of terms which describe the indirect coupling between $\boldsymbol{\psi}_{3/2}^{(n)}$ and $\boldsymbol{\psi}_{-3/2}^{(n)}$ *via* all excursions to the $\mathscr{H}_{lh}$ eigenstates.

The twofold degeneracy between $\boldsymbol{\psi}_{3/2}^{(n)}$ and $\boldsymbol{\psi}_{-3/2}^{(n)}$ will be lifted unless the matrix element $\langle \chi_n | W | \chi_n \rangle$ vanishes, which is exactly what happens when the heterostructure is symmetric with respect to the plane $z = 0$. In fact, under these circumstances

the γ's, $V_p(z)$, $-e\mathscr{A}(z)$, $\mathscr{H}_{--}$, $\mathscr{H}_{-+}$ and $\mathscr{H}_{hh}$ are even in z while W is an odd function of z. As $\chi_n(z)$ may be chosen with a definite parity, it follows that $\langle \chi_n | W | \chi_n \rangle$ vanishes. Thus, at this lower order of perturbation, the twofold degeneracy is not lifted if the heterostructure is symmetrically designed. It is possible to check that this twofold degeneracy is preserved at higher orders of perturbation.

On the other hand, if the heterostructure lacks inversion symmetry (for examples of such heterostructures see Fig. 23), the twofold degeneracy at $\boldsymbol{k}_- = \mathbf{0}$ between $\boldsymbol{\psi}^{(n)}_{\frac{1}{2}}$ and $\boldsymbol{\psi}^{(m)}_{-\frac{1}{2}}$ is already lifted at the lowest order (see equation (117)) and consequently at any order in the coupling between the unperturbed $\boldsymbol{\psi}^{(n)}$ doublet and the other $\boldsymbol{\psi}^{(m)}$ doublets.

To summarize, the lifting of the twofold (Kramers) degeneracy requires that :

i) $\boldsymbol{k}_- \neq \mathbf{0}$,

ii) $V_p(z)$ and or $-e\mathscr{A}_{xc}(z)$, $\gamma_i(z)$ lack of inversion symmetry,

iii) the spin-orbit coupling is non vanishing.

The latter condition is only implicit in our calculations as the Γ spin-orbit energies Δ_χ, Δ_β do not appear explicitly in equations (111-115). This is because they are

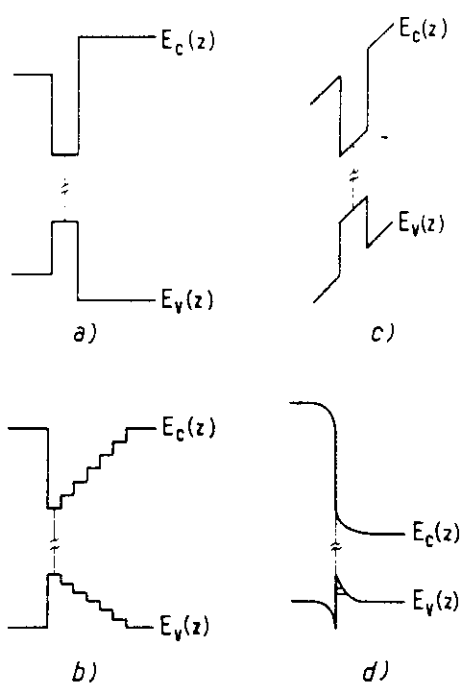

Fig. 23. — Band edges profiles of four different heterostructures lacking inversion-symmetry. a) asymmetric rectangular quantum well ; b) pseudo-sawtooth quantum well ; c) rectangular quantum well tilted by an external electric field ; d) modulation-doped p-type heterojunction.

assumed to be very large compared to the Γ_8 energies. On the other hand if both Δ_A, Δ_B vanish, the twofold degeneracy at finite $\boldsymbol{k}_{\parallel}$ is immediatly recovered. It then coincides with the spin degeneracy $\left(\sigma_z = \pm \frac{1}{2}\right)$ which obviously can not be lifted by scalar potentials like $V_p(z)$ and $-e\varphi_u(z)$.

Let us finally remark that even if the heterostructure is symmetrically designed, lifting of the Kramers degeneracy should still take place due to the lack of inversion-symmetry of the host unit cells. This effect (linear $\boldsymbol{k}$ terms in $\mathscr{H}_{\Gamma_8}$) is however small (and has been neglected in the previous analysis) compared with the lifting of the Kramers degeneracy obtained by asymmetrically designing the heterostructure. Notice also that asymmetrical situations should experimentally be the rule rather than the exception since growth processes often lead to some asymmetry between the two GaAs-Ga(Al)As interfaces.

Unless $\boldsymbol{k}_{\parallel}$ is very small, the effects of the b and c in $\mathscr{H}_{\Gamma_8}$ cannot be treated by second order perturbation but require numerical diagonalization. Again an exact solution [32] is possible if flat band conditions prevail. Other treatments [5, 33-37] which are approximate, are capable of handling band bending effects. A variational scheme has been proposed by Altarelli [2, 34] which also incorporates the differences between the γ parameters in the A and B layers. If these parameters are assumed to be the same in both kinds of layers another computational scheme becomes possible. This approximation is reasonably justified in GaAs-$Ga_{1-x}Al_xAs$ heterostructures. Let us denote by $\xi_m(z)$, $\varphi_n(z)$, the eigenfunctions of $\mathscr{H}_{hh}$ and $\mathscr{H}_{lh}$ at $\boldsymbol{k}_{\parallel} = \boldsymbol{0}$ respectively. The eigenstates of $\mathscr{H}_{\Gamma_8}$ at finite $\boldsymbol{k}_{\parallel}$ can then be expanded [5, 35, 37] in the following manner

$$\psi = \begin{bmatrix} \sum_m \alpha_m \xi_m(z) \\ \sum_n \beta_n \varphi_n(z) \\ \sum_n \beta'_n \varphi_n(z) \\ \sum_m \alpha'_m \xi_m(z) \end{bmatrix} \tag{118}$$

If the summations in equation (118) run over all the $\boldsymbol{k}_{\parallel} = \boldsymbol{0}$-heavy and light hole states, ψ is an exact solution of the problem. In practice, M heavy hole states and N light hole states are retained and $\mathscr{H}_{\Gamma_8}$ is diagonalized inside this $2(M+N)$-dimensional subspace.

To illustrate the salient features of Γ_8 in-plane dispersions, we have presented in figures 24 to 26 the results of calculations using equation (118) as the eigenfunction at finite $\boldsymbol{k}_{\parallel}$ in GaAs-$Ga_{0.7}$-$Al_{0.3}As$ single quantum wells. The expansions over m and n have been restricted to the bound heavy and light states of the quantum wells. The following parameters were used : $V_p = -0.15$ eV ; $\gamma_1 = 0.85$; $\gamma_2 = 2.1$; $\gamma_3 = 2.9$.

In addition, the calculations were performed under the axial approximation [33, 34] which amounts to replacing γ_2 and γ_3 in equation (109) by their arithmetic average. This renders the in-plane dispersions isotropic, while retaining the correct confinement energies at $\boldsymbol{k}_{\parallel} = \mathbf{0}$ [34].

Figure 24 displays the calculated valence subbands of two quantum wells (L = 100 Å and L = 150 Å respectively) under flat band conditions. As the heterostructure displays centro-symmetry with respect to the middle of the well each of the levels are twice degenerate. The dashed lines are the results obtained in the diagonal approximation ($b = c = 0$ in $\mathscr{H}_{IV}$). The mass reversal effect causes HH_1 to cross LH_1. The off-diagonal terms in $\mathscr{H}_{IV}$ replace this crossing by an anticrossing which is more pronounced at L = 150 Å than at L = 100 Å. This is because the $\boldsymbol{k}_{\parallel} = \mathbf{0}$-levels are closer in the former situation than in the latter. The mixing between the $\boldsymbol{k}_{\parallel} = \mathbf{0}$-levels is very strong, resulting in highly non-parabolic subband dispersions. In particular, one notices that the LH_1 subband displays an **electron-like** curvature in the vicinity of $\boldsymbol{k}_{\parallel} = \mathbf{0}$ [34]. This is due to the prevalent coupling between LH_1 and HH_2 (and other states of lower energies) over the repulsive coupling between HH_2 and LH_1 which pushes LH_1 towards lower energies. The electron-like mass of LH_1 is lighter in the 150 Å than in the 100 Å thick quantum well, a feature which again originates from the decreasing energy separations between the $\boldsymbol{k}_{\parallel} = \mathbf{0}$-states at larger L_z.

It is very difficult to predict general trends for the in-plane dispersion of a given heterostructure. The only model-independent conclusion is the increase in the

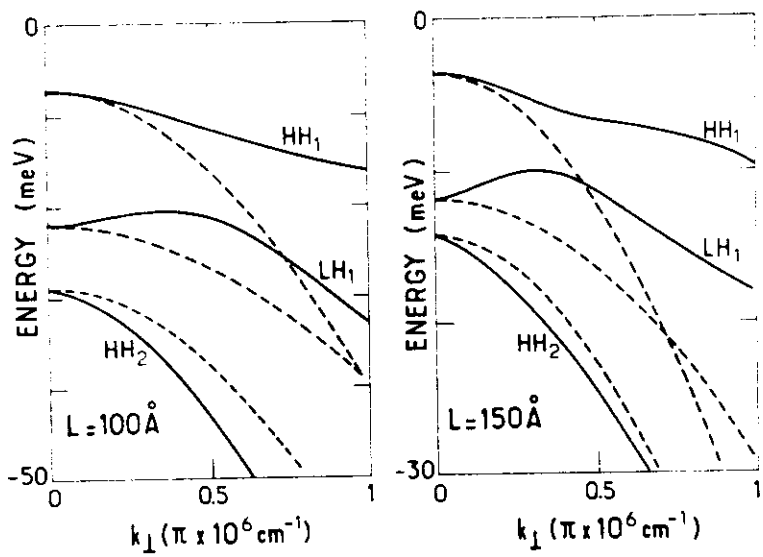

Fig. 24. — In-plane dispersion relations of the valence subbands of GaAs-$Ga_{0.7}$-$Al_{0.3}$As quantum wells (L = 100 Å and L = 150 Å respectively). The dashed lines are the subband dispersions obtained in the diagonal approximation.

HH_1 in-plane mass over the value given by the diagonal approximation : as HH_1 is the ground hole state the only result of off-diagonal pertubations is to lower its (hole) energy, thereby increasing its in-plane mass.

In figure 25 we have presented the L-dependence of the in-plane effective masses of the four lowest lying hole subbands (when existing) in GaAs-$Ga_{0.7}$-$Al_{0.3}$As quantum wells in the vicinity of $\boldsymbol{k}_{\parallel} = \mathbf{0}$. These masses were obtained by fitting the calculated in-plane dispersion to the quadratic functions of $k_{\parallel}^2$. Notice that the validity of such a quadratic expansion narrows when L increases.

To illustrate the lifting of the Kramers degeneracy in asymmetric heterostructures figure 26 shows the in-plane subbands of a GaAs-$Ga_{0.7}$-$Al_{0.3}$As quantum well (L = 100 Å) tilted by an electric field $\boldsymbol{F}$ applied parallel to $\hat{\boldsymbol{z}}$ ($F = 10^5$ V cm). Such field configurations and strengths are obtained, for instance, by inserting the quantum well into the intrinsic part of a reverse-biased p-i-n junction [38]. The centres of gravity of the two components of the various Kramer doublets follow trends which are similar to the ones already analysed in rectangular quantum wells, e.g. anticrossing between HH_1 and LH_1, electron-like behaviour of LH_1 near $\boldsymbol{k}_{\parallel} = \mathbf{0}$. The splitting due to the externally controlled inversion-asymmetry is significant : 5-6 meV for HH_1 and LH_1... This is in fact comparable in magnitude to what was calculated for modulation-doped p-type GaAs-Ga(Al)As heterojunctions [33-37]. In the latter heterostructures, the inversion-asymmetry splitting is clearly evidenced by

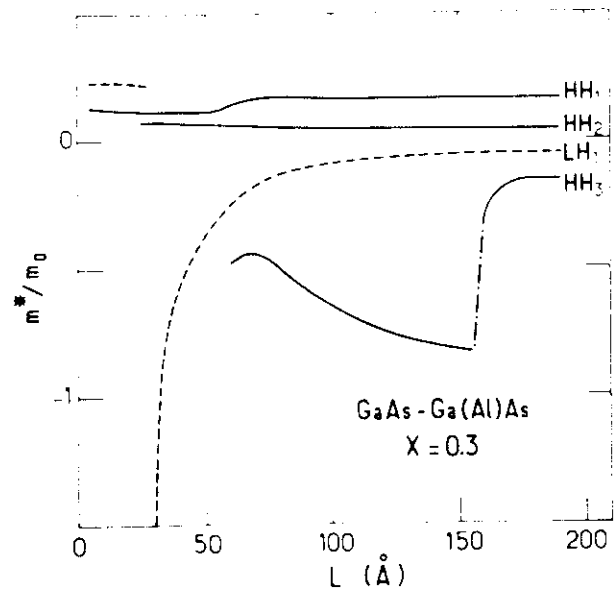

Fig. 25. — The in-plane hole effective masses near $\boldsymbol{k}_{\parallel} = \mathbf{0}$ of the four lowest lying hole subbands of GaAs-$Ga_{0.7}$-$Al_{0.3}$As quantum wells are plotted *versus* the GaAs slab thickness L.

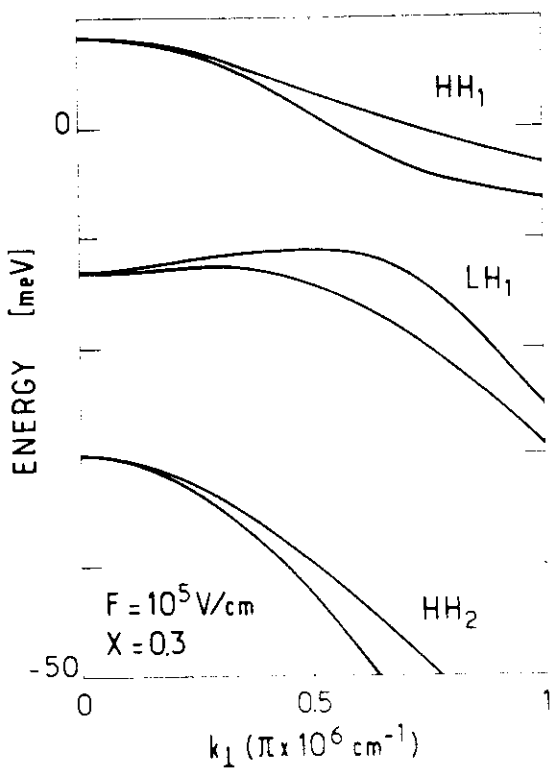

Fig. 26. — In-plane dispersions of the valence subbands of a GaAs-$Ga_{1-x}Al_xAs$ quantum well (L_z = 100 Å) subjected to an external electric field $F // z$ ($F = 10^5$ V/cm). The twofold Kramers degeneracy prevailing at $k_\parallel = 0$ is lifted at $k_\parallel \neq 0$

beating effects in the Shunikov-de Haas oscillations as well as by the existence of two hole effective masses pertaining to the HH_1 doublet.

The study of the in-plane dispersion relations in heterostructures is presently being very actively pursued both experimentally and theoretically. We wish to point out that, apart from the numerical difficulties linked to the complicated nature of the valence Hamiltonian, the lack of knowledge of **bulk** valence parameters often makes it difficult to obtain precise results. Even in the most studied GaAs-Ga(Al)As system, the γ parameters of the Ga(Al)As alloys have not, to our knowledge, been measured accurately. *A fortiori*, in less studied systems like $Ga_{0.47}In_{0.53}As$-InP, GaSb-AlSb, $Ga_{0.47}In_{0.53}As$-$Al_{0.48}In_{0.52}As$, HgTe-CdTe, the knowledge of these parameters is even more questionable. This casts doubts on the quantitative reliability of valence subband calculations, although qualitatively the gross features are relatively well understood.

Appendix A.

Boundary conditions and stationary states.

Let us consider a Ben Daniel-Duke Hamiltonian for electrons

$$\mathcal{H} = \frac{1}{2} p_z \frac{1}{m(z)} p_z + V_c(z) + \frac{\hbar^2 k_t^2}{2m(z)} \tag{A1}$$

where :

$$m(z) = \begin{cases} m_a & z > 0 \\ m_b & z < 0 \end{cases} \qquad V_c(z) = \begin{cases} 0 & z > 0 \\ V_c & z < 0 \end{cases} \tag{A2}$$

We are interested in checking the validity of the two boundary conditions for $\frac{\partial \psi}{\partial z}$

$$\frac{\partial \psi}{\partial z} \text{ continuous or } \frac{1}{m(z)} \frac{\partial \psi}{\partial z} \text{ continuous} \tag{A3}$$

given that the envelope function $\psi(z)$ is continuous everywhere.

Let us consider the time derivative of the probability amplitude

$$\frac{\partial \rho}{\partial t} = \frac{\partial}{\partial t} \left| \psi^*(z, t)\, \psi(z, t) \right| \tag{A4}$$

By using the Schrödinger equation

$$i\hbar \frac{\partial \psi(z, t)}{\partial t} = H \psi(z, t) \tag{A5}$$

we easily find that

$$\frac{\partial \rho}{\partial t} = \frac{i\hbar}{2} \frac{\partial}{\partial z} \left\{ \psi^*(z, t) \frac{1}{m(z)} \frac{\partial \psi}{\partial z}(z, t) - \psi(z, t) \frac{1}{m(z)} \frac{\partial \psi^*}{\partial z}(z, t) \right\} \tag{A6}$$

In a stationary state $\psi(z, t)$ factorizes into

$$\psi(z, t) = \psi(z) \exp\left(- \frac{i\, \varepsilon_n t}{\hbar} \right) \tag{A7}$$

where ε_n is the eigenenergy. Consequently $\frac{\partial \rho}{\partial t}$ vanishes, which leads to :

$$G(z) = \psi^*(z) \frac{1}{m(z)} \frac{\partial \psi}{\partial z}(z) - \psi(z) \frac{1}{m(z)} \frac{\partial \psi^*}{\partial z}(z) = \text{constant} \tag{A8}$$

Let us apply the conservation of $G(z)$ on each side of the A-B interface. We obtain :

$$\psi^*(0^-)\frac{1}{m_B}\frac{\partial\psi}{\partial z}(z=0^-) - \psi(0^-)\frac{1}{m_B}\frac{\partial\psi}{\partial z}(z=0^-) =$$
$$\psi^*(0^+)\frac{1}{m_A}\frac{\partial\psi}{\partial z}(z=0^+) - \psi(0^+)\frac{1}{m_A}\frac{\partial\psi}{\partial z}(z=0^+) \qquad \text{(A9)}$$

It can be seen that the boundary conditions

$$\psi(0^-) = \psi(0^+) \;;\; \frac{1}{m_B}\frac{\partial\psi}{\partial z}(z=0^-) = \frac{1}{m_A}\frac{\partial\psi}{\partial z}(z=0^+) \qquad \text{(A10)}$$

are compatible with (A9), while

$$\psi(0^-) = \psi(0^+) \;;\; \frac{\partial\psi}{\partial z}(z=0^-) = \frac{\partial\psi}{\partial z}(z=0^+) \qquad \text{(A11)}$$

do not ensure that (A9) is fulfilled.

Consequently the "traditional" boundary conditions (A11) have to be discarded for Ben Daniel-Duke problems since they do not ensure the conservation of $G(z)$ and ultimately the stationary nature of the eigenstates.

In the case of a multiband Kane Hamiltonian with remote band effects included up to the second order in k (Eq. (20)), the same kind of reasoning can be made. The only difference is that $\rho(z)$ should be written

$$\rho(z) = \sum_i \chi_i^*(z,z)\,\chi_i(z,z) \qquad \text{(A12)}$$

where i labels the band edges which are included in the analysis and $\chi_i(z,z)$ the i^{th} component of the column vector envelope function $\boldsymbol{\chi}(z,z)$. Proceeding as in (A6-A9) we find that the boundary conditions

$$\boldsymbol{\chi}(z) \;,\; \frac{\partial\boldsymbol{\chi}}{\partial z} \text{ continuous at the interfaces} \qquad \text{(A13)}$$

are incompatible with the stationary nature of the states and thus should be discarded, whereas the conditions $\boldsymbol{\chi}(z)$, $\underline{A}\,\boldsymbol{\chi}$ where $\underline{A}$ has been defined in equations (21, 22) are compatible with the stationary requirement.

Appendix B.

Coupling between light and heavy particle states due to inversion asymmetry splitting in bulk materials. Qualitative aspects.

The hosts' unit cells of actual heterostructures lack inversion-symmetry since the two atom basis of the Bravais lattice underlying the zinc-blende structure consists of two different elements (e.g. Ga and As in the case of bulk GaAs).

The effects associated with the inversion-asymmetry of the zinc-blende lattice have been thoroughly analysed in bulk materials (see e.g. [23, 39]). When combined with non zero spin-orbit coupling and the wavevector $\boldsymbol{k}$, they produce terms in the dispersion of Γ_8 bands which are linear in $\boldsymbol{k}$. When $\boldsymbol{k}$ is parallel to [111] these terms displace the maximum of the valence band from the zone centre to $[k_0, k_0, k_0]$ and raise the valence band maximum by an energy δ. In addition, with the exception of the [001] direction, the inversion asymmetry splitting removes the Kramers degeneracy of the Γ_8-related levels. The strength of the inversion-asymmetry effects is very small, more so in III-V than in II-VI compounds, to the point where a considerable scatter in the published values of δ and k_0 exists in all the III-V materials. A value of $\delta = 1$ meV seems to be an upper bound.

Our purpose in this Appendix is to discuss some of the effects of the host inversion asymmetry on the Γ_8-related heterostructures states. A more complete analysis has already been given by Bychkov and Rashba [40] using the envelope function framework and by Schulman and Chang [6] using the tight-binding approach. For the sake of simplicity let us assume that parabolic Γ_8 bands exist in the hosts, that the growth direction is [001] and that $\boldsymbol{k}_\perp = (k_x, k_y) = \boldsymbol{0}$. We shall also neglect the eventual differences in the inversion-asymmetry constants of the different kinds of layers. Under these assumptions the Hamiltonian for Γ_8-related levels becomes:

$$\mathcal{H}_{\Gamma_8} = \begin{bmatrix} \frac{1}{2m_0} p_z(\gamma_1 - 2\gamma_2) p_z + V_p(z) & \alpha p_z & 0 & 0 \\ \alpha^* p_z & -\frac{1}{2m_0} p_z(\gamma_1 + 2\gamma_2) p_z + V_p(z) & 0 & 0 \\ 0 & 0 & \frac{1}{2m_0} p_z(\gamma_1 + 2\gamma_2) p_z + V_p(z) & \alpha p_z \\ 0 & 0 & \alpha^* p_z & \frac{1}{2m_0} p_z(\gamma_1 - 2\gamma_2) p_z + V_p(z) \end{bmatrix} \tag{B1}$$

In (B1) the energy zero has been taken at the Γ_8 point in the A material. γ_1 and γ_2 are Luttinger parameters which eventually take different values in A and B layers, and the terms in αp_z are the inversion-asymmetry contributions to the Γ_8 Hamiltonian [23, 39].

Despite our $\boldsymbol{k}_\perp = \boldsymbol{0}$ assumption, the heterostructure eigenstates are no longer eigenstates of J_z if α, i.e. the inversion-asymmetry, is nonvanishing. (B1) shows that the $m_J = \pm \frac{3}{2}$ components are in fact admixed with the $m_J = \mp \frac{1}{2}$ components. The form of the coupling term αp_z also indicates that the inversion-asymmetry contributions will admix light and heavy particle states, which at $\alpha = 0$ are of opposite parities. For instance, in the case of a single rectangular quantum well, the HH_2 state will be coupled to the LH_1 state.

Finally, we notice in (B1) that the eigenstates will remain twice degenerate (Kramers degeneracy) as the 4×4 Hamiltonian has been split into two identical and uncoupled blocks. This decoupling is no longer valid if $\boldsymbol{k}_\perp \neq \boldsymbol{0}$ and/or if the growth occurs in a symmetry direction lower than [001].

Exact solutions of (B1) exist if $V_p(z)$ is piecewise constant. The eigenstates of (B1) can be written as linear combinations of bulk solutions in the A and B layers. The matching conditions at the hetero-interfaces with $\alpha \neq 0$ are the same as those obtained with $\alpha = 0$ since, by integrating (B1) across an interface, the α-dependent contributions amount to re-writing the continuity of the envelope functions. By using the appropriate boundary conditions at large $|z|$ (Bloch theorem in the case of superlattices, exponential decay in the case of quantum wells), one ends up with a transcendental equation linking the energy ε to the corresponding wavevectors k_A, k_B in each kind of layer.

Bearing in mind a qualititative estimate of the inversion-asymmetry effects, let us consider a single GaAs-Ga(Al)As rectangular quantum well. At $\alpha = 0$, the eigenstates of $\mathscr{H}_{\Gamma_8}$ are either the heavy hole states HH_n, each twice degenerate, or the light hole states LH_n, which are also each twice degenerate. Owing to the mass ratio $\dfrac{\gamma_1 - 2\gamma_2}{\gamma_1 + 2\gamma_2} > 4$ in GaAs it is easy to work out that at least two decoupled states may be degenerate if $\alpha = 0$; namely HH_2 and LH_1. In fact, $HH_2 < LH_1$ in thick quantum wells whereas in narrow wells ($L \to 0$) HH_2 fades away in the valence continuum while LH_1 remains bound in the well. Thus, for certain critical thickness L_c, HH_2 and LH_1 are degenerate at the zeroth order in α.

To qualitatively analyse the α-induced coupling at $L = L_c$, we diagonalize the inversion asymmetry contribution between HH_2 and LH_1, while neglecting all the other α-induced couplings between these two states and LH_n, HH_m. We obtain a lifting of the degeneracy at $L = L_c$ which is given by

$$\Delta\varepsilon = 2\,|\langle HH_2|\alpha p_z|LH_1\rangle| \tag{B2}$$

For an order of magnitude estimate we use

$$\langle z|HH_2\rangle = \sqrt{\frac{2}{L_c}}\sin\left(\frac{2\pi z}{L_c}\right) \tag{B3}$$

$$\langle z|LH_1\rangle = \sqrt{\frac{2}{L_c}}\cos\left(\frac{\pi z}{L_c}\right) \tag{B4}$$

and obtain :

$$\Delta\varepsilon = \frac{16}{3}\,\alpha\,\frac{\hbar}{L_c} \tag{B5}$$

The order of magnitude of α is now related to the quantity δ, which is the shift of the top of the valence band in bulk GaAs by

$$\alpha \sim \sqrt{\frac{2\delta}{(\gamma_1 - 2\gamma_2)\,m_0}} \tag{B6}$$

which gives

$$\Delta\varepsilon \sim \frac{16}{3\pi}\sqrt{\delta HH_2} \tag{B7}$$

i.e. $\Delta\varepsilon \sim$ few meV's.

Conclusions qualitatively similar to those obtained in this analysis were reached by Schulman and Chang [6] by means of empirical tight binding calculations. In such a model, the inversion-asymmetry splitting is automatically taken into account due to the difference in the atomic wavefunctions of the anions and cations from which the heterostructure states are built.

References

[1] S.R. White and L.J. Sham, *Phys. Rev. Lett.* **47** (1981) 879.

[2] M. Altarelli, *Phys. Rev.* **B28** (1983) 842 ; *Physica* **117 & 118 B** (1983) 747.

[3] M.F.H. Schuurmans and G.W.'t Hooft, *Phys. Rev.* **B31** (1985) 8041.

[4] G. Bastard, *Phys. Rev.* **B24** (1981) 5693 ; *Phys. Rev.* **B25** (1982) 7584.

[5] G. Bastard and J.A. Brum in *Quantum Well Structures, Physics and Applications, IEEE J. Quant. Electr.* **QE22** (1986) 1625.

[6] J.N. Schulman and Yia-Chung Chang, *Phys. Rev.* **B24** (1981) 4445 ; *Phys. Rev.* **B31** (1985) 2056.

[7] Yia-Chung Chang and J.N. Schulman, *J. Vac. Sci. Technol.* **21** (1982) 540.

[8] M. Jaros and K.B. Wong, *J. Phys.* **C17** (1984) L 765.

[9] M. Jaros, K.B. Wong and M.A. Gell, *Phys. Rev.* **B31** (1985) 1205.

[10] see e.g. M. Quillec, L. Goldstein, G. Le Roux, J. Burgeat and J. Primot, *J. Appl. Phys.* **55** (1984) 2904.

[11] see e.g. J.H. Neave, P.J. Dobson, B.A. Joyce and J. Zhang, *Appl. Phys. Lett.* **47** (1985) 100.

J.M. van Hove, C.S. Lent, P.R. Pukite and P.I. Cohen, *J. Vac. Sci. Technol.* **B1** (1983) 741.

[12] G.C. Osbourn, *J. Vac. Sci. Technol.* **B1** (1983) 379.

[13] P. Voisin in *Two dimensional Systems, Heterostructures and Superlattices* edited by G. Bauer, F. Kuchar and H. Heinrich, Springer Series in *Solid State Sci.* **53** (Springer Verlag, Berlin) 1984, p. 192.

[14] J.Y. Marzin in *Heterojunctions and Semiconductor Superlattices* edited by G. Allan, G. Bastard, N. Boccara, M. Lannoo and M. Voos (Springer Verlag, Berlin) 1986, p. 161.

[15] J.N. Schulman and T.C. Mc Gill in *Synthetic Modulated Structure Materials* edited by L.L. Chang and B.C. Giessen (Academic Press, New York) 1984.

[16] see e.g. E.J. Fantner and G. Bauer in *Two Dimensional Systems, Heterostructures and Superlattices* edited by G. Bauer, F. Kuchar and H. Heinrich, Springer Series in *Solid State Sci.* **53**, p. 207 (Springer Verlag, Berlin) 1984.

[17] W. Harrison, *J. Vac. Sci. Technol.* **14** (1977) 1016 ; *J. Vac. Sci. Technol.* **B3** (1985) 1231.

[18] W.R. Frensley and H. Kroemer, *Phys. Rev.* **B16** (1977) 2642.

[19] J. Tersoff, *Phys. Rev.* **B30**, 4874 (1984) ; *Phys. Rev. Lett.* **52** (1984) 465 ; *Phys. Rev.* **B32** (1985) 6968.

[20] G. Duggan, *J. Vac. Sci. Technol.* **B3** (1985) 1224.

[21] H. Kroemer, *Surf. Sci.* **132** (1983) 543 ; *J. Vac. Sci. Technol.* **B2** (1984) 433 and in *Molecular Beam Epitaxy and Heterostructures* edited by L.L. Chang and K. Ploog (Martinus Nijhoff, Dordrecht) 1985, p. 331.

[22] J.M. LUTTINGER, *Phys. Rev.* **102** (1956) 1030.
[23] G.L. BIR and G.E. PIKUS *Symmetry and Strain-induced Effects in Semiconductors* (Wiley, New York) 1974.
[24] G. DRESSELHAUS, A.F. KIP and C. KITTEL, *Phys. Rev.* **98** (1955) 368.
[25] D.J. BEN DANIEL and C.B. DUKE, *Phys. Rev.* **152** (1966) 683.
[26] see e.g. M.H. WEILER in *Semiconductor and Semimetals* vol. 16 edited by R.K. Willardson and A.C. Beer (Academic Press, New York) 1981.
[27] Y. GULDNER, G. BASTARD, J.P. VIEREN, M. VOOS, J.P. FAURIE and A. MILLION, *Phys. Rev. Lett.* **51** (1983) 907.
[28] YIA-CHUNG CHANG, J.N. SCHULMAN, G. BASTARD, Y. GUELDNER, M. VOOS, *Phys. Rev.* **B31** (1985) 2557.
[29] Y.R. LIN LIU and L.J. SHAM, *Phys. Rev.* **B32** (1985) 5561.
[30] see e.g. L. ESAKI in *Narrow Gap Semiconductors. Physics and Applications Lecture Notes Phys.* **133** (Springer Verlag, Berlin) 1980.
[31] S.S. NEDOREZOV, *Sov. Phys. Sol. State* **12** (1971) 1814.
[32] J.M. BERROIR, 1985, unpublished
[33] U. EKENBERG and M. ALTARELLI, *Phys. Rev.* **B30** (1984) 3569.
[34] M. ALTARELLI in *Semiconductor Superlattices and Heterojunctions*, edited by G. Allan, G. Bastard, N. Boccara, M. Lannoo and M. Voos (Springer Verlag, Berlin) 1986, p. 12.
[35] D.A. BROIDO and L.J. SHAM, *Phys. Rev.* **B31** (1985) 888.
[36] E. BANGERT and G. LANDWEHR, *Superlattices and Microstructures* **1** (1985) 363.
[37] T. ANDO, *J. Phys. Soc. Japan* **54** (1985) 1528.
[38] D.A.B. MILLER, D.S. CHEMLA, T.C. DAMEN, A.C. GOSSARD, W. WIEGMANN, T.H. WOOD and A.C. BURRUS, *Phys. Rev.* **B32** (1985) 1043.
[39] E.O. KANE, *J. Phys. Chem. Sol.* **1** (1957) 249.
[40] YU. A. BYCHKOV and E.I. RASHBA in the *Proceedings of the 17th International Conference on the Physics of Semiconductors*, San Francisco (1984) edited by J.D. Chadi and W.A. Harrison (Springer Verlag) 1985, p. 321.